Leveraging Millimiter Wave Communications for Effective Remote Sensing

A Dissertation Presented for the

Doctor of Philosophy

Degree

The University of Tennessee, Knoxville

Zhiyang Zhang

August 2024

© by Zhiyang Zhang, 2024
All Rights Reserved.

Acknowledgments

First and foremost, I would like to express my deepest gratitude to my academic advisor, Prof. Husheng Li. His immense knowledge and endless curiosity illuminate and guide me to find interesting research fields and bear fruit. I could not finish my PhD study without your help. Thank you so much for your continuous support and patience.

I would like to thank my advisor, Prof. Seddik M. Djouadi. Thank you for helping me finish my PhD study. Your optimism and encouragement give me true grit to face difficulties, not only in study, but also in life.

Besides my advisors, I would like to thank the rest of my thesis committee, Prof. Aly Fathy and Prof. Weizi Li. They have provided me extensive professional guidance and encouragement for my thesis.

I would like to express my sincere gratitude to all my collaborators, Yawen Fan, Jingchao Bao, Liang Li, Yifan Wang, and Mustafa Sadiq. It was a pleasure to collaborate with and to learn from you all.

Last but not the least, I would like to thank my parents. Thank you for raising me up and supporting me materially and spiritually. You are my heroes.

Abstract

Millimeter wave (mmWave) is a promising technique in the 5th generation of cellular communications due to its large bandwidth and thus unprecedentedly high data transmission rate. To study the characteristics of mmWave and evaluate various algorithms, we build a high directional mmWave communication testbed.

The first topic of this thesis consists of two parts. The first one seeks to track a single object by using blockage phenomenon. Algorithms to capture the moving object are proposed. Detailed experiments and numerical simulations are compared with actual GPS trajectory to demonstrate the accuracy of the proposed solutions. In the second part, we formulate the multiple moving objects problem and then convert it to an intuitive geometric problem. Numerical results have shown that the proposed algorithms are promising and may find potential applications in practice.

The second topic in this thesis leverages the mmWave communications in the outdoor environment to estimate wind velocity. A force and motion model is proposed and the Doppler effect is considered to prove the causation between wind velocity and frequency difference. Then we propose a mathematical model and algorithms to estimate wind velocity in one receiver with multiple beams in different directions. We carry out experiments in the 60GHz band to demonstrate the theoretical prediction, with the outcome matching the theoretical model. Numerical simulations are carried out to evaluate the performance of wind velocity estimation.

The third topic studies optical-like characteristics of mmWave. The mechanism of oscillation is exhaustively illustrated. We propose an algorithm using its periodic

trends and a simulation with real measurements testifies its accuracy in short distance. We carry out experiments in our testbed to verify the phenomenons of reflection and diffraction. Then we propose a tracking algorithm based on the Kalman Filter.

Contents

1 Introduction **1**

1.1 Motivation 1

1.1.1 mmWave in Telecommunications 2

1.1.2 Overcoming Challenges 3

1.1.3 Future Prospects 3

1.2 Related Work 4

1.2.1 Strategies to Mitigate Blockage Effects 4

1.2.2 Using Blockage to Characterize Interferers in mmWave Communication 7

1.2.3 Interferer Tracking 9

1.2.4 Conclusion 11

1.3 My Work 12

1.4 Outline of this Thesis 13

2 Background of mmWave **15**

2.1 Millimeter Wave 15

2.1.1 Early Research and Development 15

2.1.2 Advances in Technology 16

2.2 Characteristics of mmWave 17

2.2.1 Highly Directional 17

2.2.2 Propagation Loss 17

2.2.3 Atmospheric Effect . . . 18
2.2.4 Blockage . . . 20

3 Object Tracking via Blockage **22**
3.1 Introduction . . . 22
3.2 Experiments on Blocking Effect . . . 24
3.2.1 Testbed . . . 24
3.2.2 Procedure . . . 27
3.2.3 Scenarios and Results . . . 27
3.3 Single Object Tracking . . . 32
3.3.1 Problem Formulation . . . 32
3.3.2 Shortest Path Criterion . . . 32
3.3.3 Minimum Velocity Variance Criterion . . . 34
3.3.4 Performance Analysis . . . 37
3.3.5 Numerical Simulations . . . 42
3.3.6 Conclusion . . . 44
3.4 Multiple Objects Tracking . . . 47
3.4.1 Problem Formulation . . . 47
3.4.2 Geometric Heuristics . . . 49
3.4.3 Recognition Algorithm . . . 49
3.4.4 Performance Analysis . . . 51
3.4.5 Numerical Simulations . . . 54
3.4.6 Conclusion . . . 54

4 Wind Sensing **57**
4.1 Introduction . . . 57
4.2 Doppler Shift and Amplitude Modulation . . . 59
4.2.1 Force and Motion Model . . . 59
4.2.2 Doppler Shift . . . 60
4.2.3 Amplitude Modulation . . . 61

4.3 Wind Velocity Estimation . . . 63
4.3.1 Mathematical Model . . . 63
4.3.2 Algorithm . . . 65
4.4 Experiment and Simulations . . . 66
4.4.1 Testbed . . . 66
4.4.2 Experiment Procedure . . . 66
4.4.3 Data Processing . . . 68
4.4.4 Experimental Results . . . 70
4.4.5 Numerical Simulation . . . 70
4.5 Conclusion . . . 74

5 Optical-like Properity Study of mmWave **75**
5.1 Oscillation . . . 75
5.1.1 Tracking Algorithm . . . 77
5.1.2 Verification . . . 79
5.2 Reflection . . . 80
5.2.1 Experiment procedure . . . 80
5.2.2 Problem Formulation . . . 82
5.2.3 Tracking Algorithm based on Kalman Filter . . . 84
5.2.4 Simulation and Analysis . . . 86
5.2.5 Conclusion . . . 86
5.3 Diffraction . . . 88
5.3.1 Single-slit Diffraction . . . 88
5.3.2 Double-slit Interference . . . 90
5.3.3 Conclusion . . . 90

6 Conclusions and Future Work **93**
6.1 Conclusions . . . 93
6.2 Future Work . . . 94

Bibliography **95**

Vita **107**

List of Tables

3.1 Hardware Testbed Components 25

5.1 Parameters measurements. 81

5.2 Comparison of actual and estimated values. 81

List of Figures

2.1 Frequency and Wavelength of mmWave 19

2.2 Effect of oxygen and water vapor on wave propagation in different frequencies 19

3.1 An illustration of the millimeter wave blocking based tracking, using the picture in *Entrapment*. 25

3.2 Input Signal. 26

3.3 External Clock. 26

3.4 HMC6300 Motherboard/TXModule Assembly with USB, DC Power, Antenna, External Clock and I/Q Cables Installed. 28

3.5 HMC6301 Motherboard/RXModule Assembly with USB, DC Power, Antenna, External Clock and I/Q Cables Installed. 28

3.6 The experiment setup 29

3.7 Live picture of the experiment. 29

3.8 SNR varies with distance in static blockage scenario. 31

3.9 The change of amplitude when a person passes the LoS. 31

3.10 SNR varies with distance in dynamic blockage scenario. 31

3.11 Coordinates and speeds in estimated path. 35

3.12 Comparison between the two criteria. 35

3.13 An illustration of the simplified model of trajectory. 40

3.14 Illustration of error between the arc and chord 40

3.15 Illustration of the covering and geometry in the proof of Theorem 3.2 43

3.16 DP estimation, GD estimation and actual trajectories 43
3.17 Estimation error in terms of communication link density 45
3.18 Computation cost in terms of communication link density 45
3.19 Estimation error in terms of average communication link length . . . 45
3.20 Relative estimation error in terms of average communication link length 46
3.21 Histogram of estimation errors 46
3.22 The two stages of trajectory tracking for multiple objects. 48
3.23 Distance range in terms of passing time in two objects scenario. . . . 50
3.24 Cones of different moving objects. 50
3.25 Case 1 53
3.26 Case 2 53
3.27 Case 3 53
3.28 Case 4 53
3.29 Four cases of the scenario of two objects. 53
3.30 Recognition rate in term of starting time difference. 55
3.31 Recognition rate in term of speed ratio. 55

4.1 Force and motion illustration. 64
4.2 Two antennas and wind velocity. 64
4.3 Analog Devices EK1HMC6350 board with antenna. 67
4.4 DJI E1200 standard tuned propulsion system. 67
4.5 Live picture of the experiment. 69
4.6 The experiment setup 69
4.7 Curve fitting for evaluating the frequency oscillation. 71
4.8 Frequency shifts in the demodulated signal over time. 71
4.9 Frequency shift in finer time scale. 72
4.10 Frequency variance in different wind speeds and directions. 72
4.11 Mean squared error of wind direction estimation. 73
4.12 Mean squared error of wind speed estimation. 73

5.1 Variation and oscillations of signal strength before and after a blockage. 76
5.2 Mechanism of oscillations before and after the blockage. 76
5.3 Four possible solutions to Eq. (5.8). 81
5.4 Experiment procedure. 83
5.5 SNR in terms of angle. 83
5.6 Actual and filtered trajectories. 87
5.7 Error in term of average sample rate. 87
5.8 Error in term of average sample rate. 87
5.9 Live picture of single-slit. 89
5.10 Single-slit diffraction experiment setup. 89
5.11 Case 1: b=10mm. 91
5.12 Case 2: b=20mm. 91
5.13 Double-slit interference experiment setup. 91
5.14 Double-slit interference experiment results. 91

Chapter 1

Introduction

1.1 Motivation

mmWave technology plays a crucial role in the deployment of 5G networks. It offers significantly higher data transfer rates compared to traditional microwave frequencies, enabling faster and more reliable wireless communication. With the exponential growth of data usage and the demand for high-speed internet, mmWave is essential for meeting these requirements. While telecommunications is a major driver, mmWave technology has promising applications in other fields as well:

- **High-Speed Internet Access**: mmWave technology has the potential to revolutionize broadband internet access, especially in urban areas where traditional wired infrastructure may be limited or expensive to deploy. By using mmWave for fixed wireless access, providers can offer gigabit-speed internet to homes and businesses without the need for extensive cabling. [4]

- **Automotive Industry**: mmWave radar systems are used in advanced driver-assistance systems (ADAS) for collision avoidance, adaptive cruise control, and autonomous driving [4].

- **Security and Surveillance**: mmWave scanners provide non-invasive, high-resolution imaging for security checks at airports and other sensitive areas. mmWave technology is employed in security screening systems, particularly in airports, to detect concealed objects on individuals [86]. It offers superior imaging capabilities compared to traditional metal detectors, providing security personnel with detailed scans for enhanced threat detection.

- **Healthcare**: mmWave imaging systems offer high-resolution capabilities for medical diagnostics and treatment monitoring. In the field of medical imaging, mmWave technology has shown promise for applications such as breast cancer detection and monitoring. Its ability to penetrate tissues and produce high-resolution images makes it a valuable tool for healthcare professionals [68].

- **Industrial Applications**: mmWave sensors are used in various industrial applications for distance measurement [54], object detection [62], and depth sensing [12]. They offer precise and reliable performance in harsh environments, making them suitable for use in manufacturing, robotics, and automation.

Overall, mmWave technology's high bandwidth, short wavelengths, and ability to penetrate various materials make it a versatile and valuable technology with numerous practical applications across different industries.

1.1.1 mmWave in Telecommunications

In recent decades, the interest in mmWave technology has shifted towards its potential in telecommunications. The ever-increasing demand for high-speed data transmission has driven the exploration of mmWave frequencies for wireless communication. The development of 5G technology has been a pivotal moment in this journey. 5G networks aim to provide significantly higher data rates, reduced latency, and increased capacity compared to previous generations of wireless technology. To achieve these goals, mmWave frequencies are being utilized to provide the necessary

bandwidth. However, the adoption of mmWave technology in 5G networks poses several challenges, including high atmospheric attenuation, limited range, and the need for advanced beam-forming techniques to ensure reliable communication.

1.1.2 Overcoming Challenges

To address the challenges associated with mmWave propagation, researchers have focused on several key areas:

- Antenna Design: Development of sophisticated antenna arrays capable of beamforming and beam steering to maintain strong signal connections despite the short-range and high directionality of mmWave signals [87].
- Semiconductor Technology: Advances in semiconductor materials and fabrication techniques have led to the creation of more efficient and higher power mmWave transceivers [37].
- Signal Processing: Enhanced signal processing algorithms to mitigate the effects of interference and signal degradation over short distances [28].
- Material Studies: Investigations into materials that can efficiently guide and reflect mmWave signals, which are critical for building mmWave-compatible infrastructure [2].

1.1.3 Future Prospects

As mmWave technology continues to evolve, it promises to revolutionize various industries by enabling ultra-fast data transmission, enhancing the performance of radar and imaging systems, and supporting the development of next-generation wireless networks. Continued research and innovation will be essential to fully realize the potential of mmWave technology and to overcome the remaining technical challenges.

The integration of mmWave technology into everyday applications will likely lead to transformative changes in how we communicate, travel, receive medical care, and secure our environments, making it a cornerstone of future technological advancements.

1.2 Related Work

In this section, we list some of the existing research that related to the topic in this thesis.

1.2.1 Strategies to Mitigate Blockage Effects

To address the challenges posed by blockage in mmWave communication, several strategies can be employed:

- **Advanced Beamforming Techniques**: Beamforming involves directing the signal in a narrow beam towards the receiver, rather than broadcasting it in all directions. This helps to focus the energy and maintain a strong signal even in the presence of obstacles. Advanced beamforming techniques can dynamically adjust the direction of the beam to find the best path to the receiver, bypassing obstacles [55, 57]. These techniques can also help in maintaining connection quality by steering beams away from obstructions and towards clear paths.

- **Densification of Base Stations**: Deploying a higher density of base stations can ensure that there are multiple possible paths for the signal to reach the receiver. This increases the likelihood of maintaining LoS and reduces the impact of any single obstruction. In urban environments, this might involve placing small cells on street furniture, buildings, and other infrastructure to create a dense network [21]. Densification helps in creating a mesh of connections, providing alternative routes for the signal and enhancing overall network reliability.

- **Use of Reflectors and Repeaters**: Reflectors can be strategically placed to bounce the signal around obstacles, maintaining a connection even when direct LoS is not possible [89]. Repeaters can receive and retransmit the signal, effectively extending its range and bypassing obstructions [50]. These devices can be crucial in indoor environments or areas with significant obstacles. For example, in a complex building layout, strategically placed reflectors can redirect signals around corners, while repeaters can boost signal strength in areas with poor coverage.

- **Adaptive Modulation and Coding**: By dynamically adjusting the modulation and coding schemes based on the quality of the signal, the system can maintain reliable communication even in the presence of blockage. Lower modulation schemes can be used to maintain connectivity at the expense of data rate when high attenuation is detected [30]. Adaptive techniques help in optimizing the use of available spectrum and maintaining communication quality under varying conditions.

- **Network Planning and Optimization**: Careful planning of the network layout, taking into account the typical movement of people and objects, can help mitigate the effects of blockage. Simulation tools can model the propagation environment and help design networks that are robust to common obstructions [51, 61]. This involves mapping the environment, identifying potential sources of blockage, and designing the network to avoid or mitigate these areas. Optimization algorithms can dynamically adjust network parameters to adapt to changes in the environment.

Research and Development Efforts

Ongoing research is focused on improving the robustness of mmWave communication in the presence of obstacles. Some of the areas of investigation include:

- **Intelligent Reflecting Surfaces (IRS)**: These are surfaces that can be electronically controlled to reflect signals in specific directions, effectively steering the beam around obstacles [11]. IRS technology allows for real-time control of the propagation environment, optimizing signal paths dynamically.

- **Machine Learning Algorithms**: Algorithms that can predict the presence and movement of obstacles and adjust the network parameters in real-time to maintain optimal performance [5, 7, 77]. Machine learning models can analyze historical data and current conditions to predict potential blockages and adapt the network configuration accordingly.

- **Hybrid Systems**: Combining mmWave with lower frequency bands to provide a fallback in case of severe blockage, ensuring continuous connectivity [72, 73]. Hybrid systems can leverage the strengths of different frequency bands to maintain robust communication in diverse environments.

Overall, while blockage presents a significant challenge for mmWave communication, a combination of advanced technologies and strategic planning can mitigate its effects, enabling the deployment of high-performance mmWave networks in various environments.

Example Scenarios

Consider a smart city equipped with mmWave technology:

- **Location Detection**: Multiple mmWave sensors are deployed across the city. Each sensor measures signal strength and attenuation patterns to detect the presence of obstacles like buildings, vehicles, and people [74]. By combining data from multiple sensors, the system can map out areas with potential blockages and adjust network parameters to maintain connectivity [27].

- **Speed Detection**: The sensors also measure Doppler shifts caused by moving objects, allowing the system to track the speed of vehicles and pedestrians. This

information is used to optimize traffic flow, enhance public safety, and improve urban mobility [35].

- **Real-Time Monitoring**: The system continuously monitors the environment, using advanced algorithms to predict and mitigate the impact of blockages. By dynamically adjusting beamforming patterns, deploying repeaters, and leveraging reflectors, the network maintains high performance and reliability despite the presence of obstacles [53].

1.2.2 Using Blockage to Characterize Interferers in mmWave Communication

Blockage can be a critical factor in characterizing interferers in mmWave communication systems. By understanding how different obstacles affect signal propagation, we can infer the presence, type, and location of potential interferers. This information is invaluable for optimizing network performance, mitigating interference, and improving overall communication reliability. Here's how blockage can be used to characterize interferers:

- **Identifying Interferers Based on Attenuation Patterns** Different materials and objects cause characteristic attenuation patterns. By analyzing these patterns, it is possible to identify the type of interferer [9, 55, 71]. For instance:
  - **Human Presence**: A sudden, temporary attenuation of 20-35 dB could indicate a person moving through the signal path.
  - **Structural Elements**: Persistent and high attenuation (40-80 dB) could suggest the presence of building materials like brick or concrete.
  - **Foliage and Vegetation**: Variable attenuation depending on weather conditions might indicate the presence of trees or plants.

- **Analyzing Signal Reflection and Diffraction** Interferers can cause reflections and diffraction, which alter the signal path. By examining these changes, the nature and position of the interferers can be deduced:
  - **Reflection Analysis**: Surfaces like walls, floors, and ceilings reflect mmWave signals. By mapping the reflections, the locations of these surfaces can be identified, indicating the presence of structures [19].
  - **Diffraction Patterns**: The lack of significant diffraction in mmWave signals (compared to lower frequencies) can help distinguish between different types of obstacles. For example, a sharp drop in signal strength without much bending around the obstacle points to large, dense objects [82].
- **Leveraging Spatial and Temporal Signal Variations** The spatial and temporal variations in signal strength can provide clues about the interferers:
  - **Spatial Analysis**: By measuring signal strength at different locations, it is possible to create a map of attenuation hotspots, indicating where interferers are located [58].
  - **Temporal Analysis**: Changes in signal strength over time can indicate moving interferers. For example, if the signal periodically weakens and then returns to normal, it could suggest the presence of moving vehicles or people [24].

Practical Applications

- **Smart City** : Characterizing interferers can help in designing robust communication networks that account for the presence of buildings, vehicles, and people, ensuring reliable connectivity in urban environments [67].

- **Indoor Environments**: Understanding the impact of walls, furniture, and human movement on mmWave signals can aid in optimizing indoor wireless networks for better performance and coverage [3, 70].

- **Vehicular Networks**: Identifying and mitigating interference from other vehicles, road infrastructure, and environmental elements can enhance the reliability of vehicular communication systems [25, 31].

By leveraging the characteristics of blockage in mmWave propagation, it is possible to effectively characterize interferers in a wireless communication environment. This involves analyzing attenuation patterns, reflection and diffraction behavior, spatial and temporal signal variations, and employing advanced machine learning techniques. Such characterization helps in designing more resilient and efficient communication networks, ensuring reliable connectivity even in the presence of potential interferers.

1.2.3 Interferer Tracking

Determining the Location of the Interfere

- **Time of Flight (ToF) Measurement**: By measuring the time it takes for the signal to travel to the interferer and back, you can calculate the distance to the interferer. This is done using the equation: $t = \frac{2d}{c}$, where d is the distance, c is the speed of light, and t is the round-trip time [1].

- **Angle of Arrival (AoA) Estimation**: Using an array of antennas, you can determine the direction from which the signal arrives. By comparing the phase differences of the received signal at different antennas, you can estimate the angle of arrival. This method helps in pinpointing the direction of the interferer [1].

- **Triangulation**: By combining AoA and ToF measurements from multiple sensors or base stations, you can triangulate the exact location of the interferer.

This method requires multiple points of measurement to accurately determine the interferer's position [26].

- **Beamforming**: Advanced beamforming techniques can focus the transmitted signal in specific directions and measure the received signal's strength. By scanning the environment and noting where signal strength drops or changes, the location of the interferer can be inferred [55].

Determining the Speed of the Interferer

- **Doppler Shift Measurement**: The Doppler effect causes a shift in the frequency of the signal if the interferer is moving relative to the transmitter. By measuring the change in frequency (Δf), the speed (v) of the interferer can be calculated using the equation: $v = c\frac{\Delta f}{f_o}$ where ccc is the speed of light, Δf is the frequency shift, and f_o is the original frequency of the transmitted signal [69].

- **Range-Doppler Maps**: By combining ToF and Doppler shift measurements, you can create a range-Doppler map that shows both the distance and speed of the interferer. This technique is commonly used in radar systems [45].

- **Phase Shift Analysis**: Continuous monitoring of the phase shift of the received signal can provide information about the speed of the interferer. A moving interferer will cause a time-varying phase shift that can be analyzed to determine its velocity [76].

Practical Implementation

To practically implement these methods, the following steps and technologies are typically used:

- **Sensor Arrays**: Deploy an array of sensors or antennas to capture the transmitted and reflected signals from multiple angles and distances [88].

- **Signal Processing Algorithms**: Implement advanced signal processing algorithms to analyze ToF, AoA, Doppler shifts, and phase shifts. Algorithms such as MUSIC (Multiple Signal Classification) and ESPRIT (Estimation of Signal Parameters via Rotational Invariance Techniques) are often used for AoA estimation [44].

- **Synchronization**: Ensure that all measurement points (sensors or base stations) are synchronized in time to accurately correlate the received signals [81].

- **Data Fusion**: Fuse data from multiple sources to enhance the accuracy of location and speed estimations. This can involve combining ToF, AoA, and Doppler measurements from different sensors [79].

By leveraging techniques such as Time of Flight, Angle of Arrival, Doppler shift measurement, and advanced signal processing, it is possible to accurately determine the location and speed of an interferer from the transmitted signal. These methods are essential for applications in wireless communication, radar systems, and various smart sensing technologies.

1.2.4 Conclusion

Blockage presents a significant challenge for mmWave communication due to its reliance on line of sight and susceptibility to material-specific attenuation. However, through the use of advanced technologies such as beam-forming, network densification, reflectors, repeaters, and adaptive modulation, it is possible to mitigate these effects. Ongoing research and development efforts continue to enhance the robustness and reliability of mmWave communication systems, paving the way for their widespread adoption in various applications. By understanding and addressing the challenges posed by blockage, we can unlock the full potential of mmWave technology and ensure its successful implementation in real-world environments.

1.3 My Work

We built a mmWave testbed, carried out a series of experiments, established mathematical models, proposed corresponding algorithms, verified feasibility and analyzed performance.

- **mmWave Characteristics Investigation**
  - Built a high directional mmWave communication testbed.
  - Carried out experiments to study the impact of objects blocking mmWave signals.
  - Carried out experiments to study the Doppler effect on mmWave communication under windy circumstance.
  - Explored or verified the phenomenons of oscillation, reflection and diffraction.
- **Theoretical Models**
  - Proposed a walking trajectory model to describe human being's walking trajectory.
  - Proposed a force and motion model to estimate wind velocity.
- **Sensing Algorithms**
  - Developed two tracking algorithms based on different criteria: shortest path and minimum s variance.
  - Developed a multiple-object recognition algorithm based on geometric heuristics.
  - Developed a wind estimation algorithm based on Doppler effect.
- **Validation with Real Data:**

- Simulated the tracking algorithms using GPS-based real trajectories.
- Verified the algorithms' effectiveness and accuracy through these simulations.

1.4 Outline of this Thesis

Next, we introduce background of mmWave in chapter 2, including its definition, brief history, and main characteristics.

In chapter 3, we conducted a series experiments to investigate the blocking effect in mmWave communication. The results showed that a passing object can be detected via blockage phenomenon, while it is infeasible to locate the object precisely. Two tracking algorithms are proposed based on different hypotheses, namely shortest path and minimum velocity variance. The performance of tracking algorithms are analyzed for both a simplified model and asymptotic case. At last, the estimation of trajectory are compared with GPS based real trajectory, and shows the validity of the tracking algorithms proposed [94].

We also studied long-term tracking problems for multiple objects by leveraging the reflection-interference effect close to the LOS and the geometric image of distance-time plane, respectively. Numerical and experimental results show that the long-term trajectory estimations achieve excellent performances [90].

In chapter 4, we carried out experiments to examine the Doppler effect caused by wind in the millimeter wave band. The results showed that a frequency oscillation can be detected in the demodulated signal. We proposed an algorithm to calculate the wind velocity. We carried out experiments in the 60GHz band to demonstrate the theoretical prediction, and the outcome matches the theoretical model quite well. Numerical simulations are carried out to evaluate the performance of wind velocity estimation [92].

In chapter 5, we study some interesting characteristics of mmWave. We carry out experiments in our testbed to verify the phenomenons of oscillation [90], reflection

and diffraction. Based on experiments, we propose math models and corresponding algorithms.

We conclude in chapter 6.

Chapter 2

Background of mmWave

In this chapter, we introduce the basic concepts for the problems discussed in this thesis. The readers are encouraged to read this chapter before going to the details in the following chapters.

2.1 Millimeter Wave

Extremely high frequency (EHF) refers to the band of radio frequency between 30 to 300 gigahertz(GHz). It has wavelengths from 10 to 1 millimeter, hence radiation in this band is called **millimeter wave**, as depicted in Fig. 2.1.

The study of mmWave began more than 100 years ago, driven by the quest to explore the properties and potential applications of electromagnetic waves in this frequency range. Early investigations primarily focused on understanding the basic characteristics of mmWaves, such as their propagation behavior, interaction with materials, and potential for use in communication and radar systems.

2.1.1 Early Research and Development

The initial studies of mmWaves were largely theoretical and experimental in nature. Researchers aimed to understand the fundamental principles governing

the propagation of mmWaves and their interaction with various materials. This period saw the development of early mmWave sources and detectors, which laid the groundwork for future technological advancements.

In 1865, James Clerk Maxwell first predicted electromagnetic propagation at the speed of light [49]. After that, many concepts now well-known in microwave were developed and laid a solid foundation to mmWave research. This foundational discovery laid the groundwork for many concepts now well-known in microwave technology, which in turn provided a solid basis for subsequent mmWave research.

In 1895, J.C. Bose achieved a significant milestone by successfully transmitting and receiving 60 GHz electromagnetic waves through two intervening walls over a distance of 23 meters. His demonstration involved remotely ringing a bell and detonating gunpowder, showcasing the potential of mmWave technology. To accomplish this, Bose developed various essential millimeter-wave components, including a spark transmitter, coherer, dielectric lens, polarizer, horn antenna, and cylindrical diffraction grating. These innovations were critical in demonstrating the feasibility of using mmWaves for communication and laid the technical foundation for future advancements [20].

2.1.2 Advances in Technology

Despite these early breakthroughs, the interest in mmWave research waned with the emergence of lasers in the 1960s [20]. Lasers offered new possibilities and captured the attention of the scientific community, leading to a shift in research focus. Nevertheless, around the same time, significant funding was injected into programs aimed at developing mmWave components for use in radiometers, radars, and missile guidance systems. These efforts underscored the strategic importance of mmWave technology, particularly in military applications, where its unique properties were highly valued.

The 1970s marked a significant turning point for mmWave research with the advent of solid-state sources. These new sources provided a major boost to mmWave

technology by improving the efficiency and reliability of mmWave devices. Solid-state technology enabled the development of more compact, powerful, and cost-effective mmWave components, which in turn expanded the scope of research and development efforts. The period saw increased diversity in the applications of mmWave technology and significant technical progress, leading to the integration of mmWaves into various systems and devices.

2.2 Characteristics of mmWave

2.2.1 Highly Directional

mmWave technology is known for its excellent directionality, a characteristic resulting from its small wavelength. This small wavelength allows for the design and implementation of highly directional antenna arrays. These arrays can focus the transmitted energy into narrow beams, which can be precisely directed towards the receiving antenna. This capability provides substantial array gains and enables the synthesis of highly directional beams, offering a stark contrast to the more omnidirectional nature of traditional 4G network antennas [83]. The high directionality of mmWave signals means that interference from other sources can be significantly reduced. In mmWave communication, each beam is narrowly focused, reducing the likelihood of overlap with other beams and thereby minimizing interference. Consequently, mmWave networks are often limited by noise rather than interference, enhancing their overall performance and reliability [75]. This attribute is particularly beneficial in dense urban environments, where interference from numerous devices can be a significant issue.

2.2.2 Propagation Loss

The propagation of electromagnetic waves in free space can be mathematically characterized by the Friis transmission equation [23] 2.1:

$$P_r = P_t G_t G_r (\frac{\lambda}{4\pi})^2 d^{-n} \tag{2.1}$$

where P_r is the received power, P_t is the transmitted power, G_t and G_r are the gains of the transmitting and receiving antennas, λ is the wavelength, and d is the distance between the antennas.

Given that the wavelength (λ) of an electromagnetic wave is inversely proportional to its frequency (f), the received power is proportional to the square of the wavelength. Consequently, higher frequencies (such as those in the mmWave band) experience significantly greater free space loss compared to lower frequencies.

For instance, at a fixed distance of 100 meters, the path loss at 60 GHz is 28 dB higher than at 2.4 GHz and 42.3 dB higher than at 460 MHz. This substantial path loss presents a notable challenge for the adoption of mmWave as a new wireless communication medium. Engineers and researchers must devise strategies to mitigate these losses, such as using highly directional antennas, employing beamforming techniques, and designing network architectures that minimize the impact of propagation loss.

2.2.3 Atmospheric Effect

The propagation of mmWave signals is significantly affected by atmospheric conditions, particularly attenuation caused by gases like oxygen and water vapor. Different gases absorb electromagnetic waves at specific frequencies, leading to increased attenuation.

At 60 GHz, for example, oxygen molecules absorb a considerable amount of energy from the mmWave signal, resulting in significant attenuation. Similarly, water vapor in the atmosphere can cause attenuation at other frequencies, such as 30 GHz and 120 GHz. This effect is illustrated in Fig. 2.2, which shows the attenuation of mmWave signals at different frequencies due to atmospheric gases.

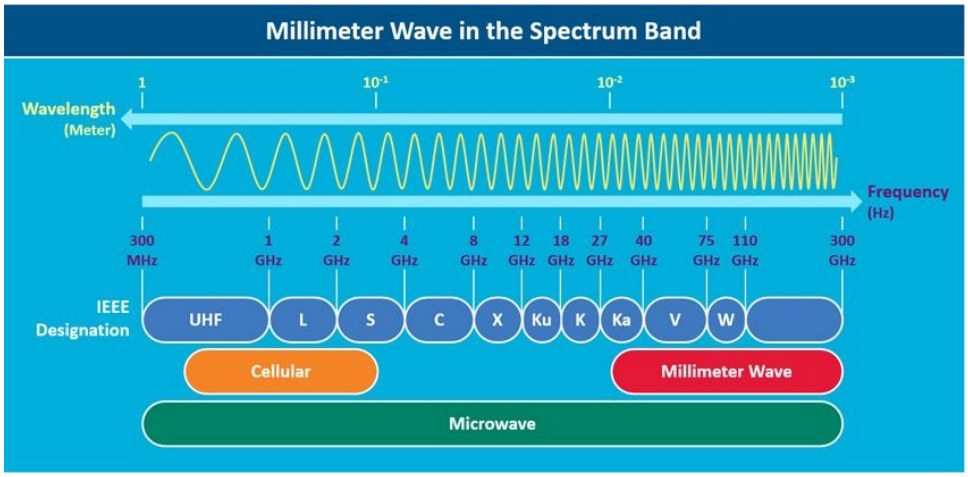


Figure 2.1: Frequency and Wavelength of mmWave

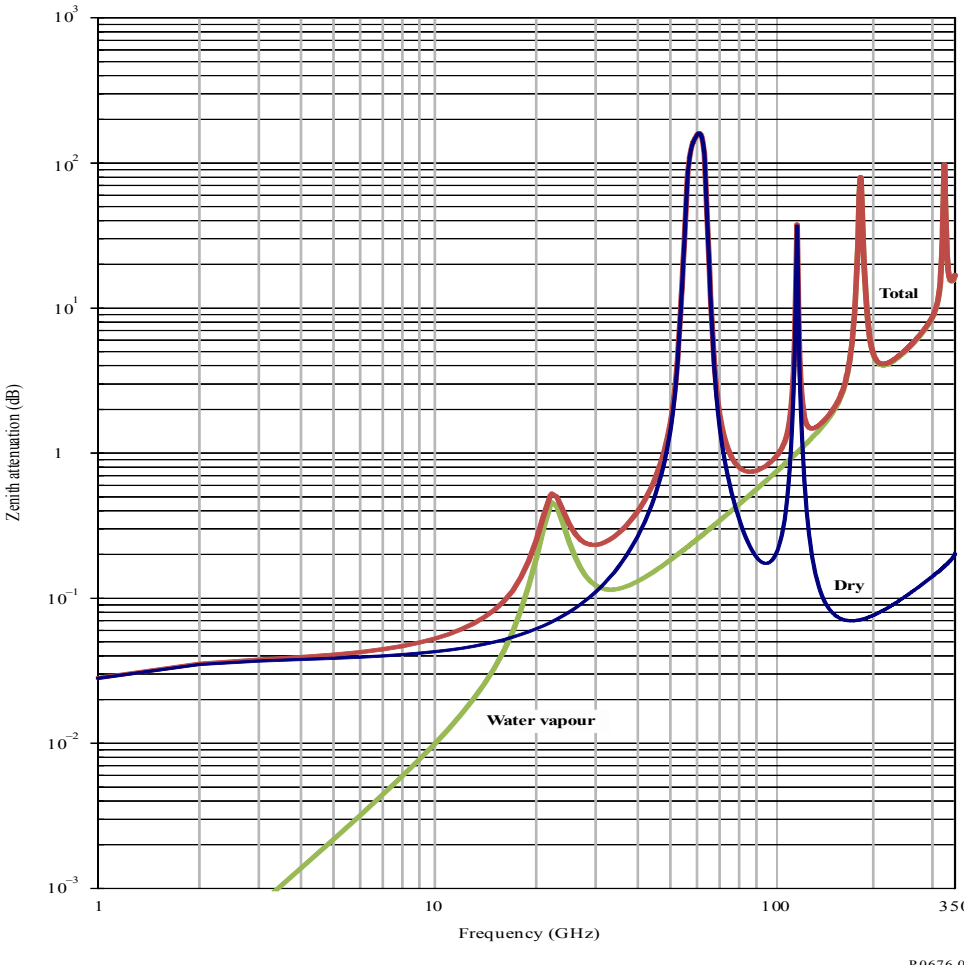


Figure 2.2: Effect of oxygen and water vapor on wave propagation in different frequencies

In dry or normal weather conditions, the presence of water vapor is relatively minor, and its impact on mmWave propagation is limited. However, during adverse weather conditions such as rain, snow, hail, or fog, water vapor becomes a major factor in attenuation. These conditions can dramatically increase the total attenuation of mmWave signals, affecting the reliability and performance of mmWave communication systems [22, 63].

Due to the weather-dependent nature of atmospheric attenuation, significant research efforts are dedicated to understanding and mitigating these effects. Techniques such as adaptive modulation, error correction, and dynamic beam steering are employed to compensate for the varying attenuation levels caused by atmospheric conditions. Additionally, network planning and deployment strategies must consider the impact of weather on mmWave propagation to ensure robust and reliable communication.

Overall, while mmWave technology offers substantial benefits in terms of bandwidth and data rates, its practical implementation requires addressing challenges related to propagation loss and atmospheric effects. Ongoing research and technological advancements continue to improve the feasibility and performance of mmWave communication systems, paving the way for their widespread adoption in various applications.

2.2.4 Blockage

A significant downside of mmWave technology is its strong susceptibility to blockage. Objects in the propagation path can cause severe channel attenuation, often resulting in losses of 10 dB or more. This poses a critical challenge in wireless communications, particularly for maintaining reliable links.

Impact of Blockage on mmWave Communication

1 **Line of Sight (LoS) Dependence**: mmWave communication heavily relies on a clear line of sight (LoS) between the transmitter and receiver. Any obstruction in the signal path can result in substantial signal degradation or complete loss of connectivity. Unlike lower frequency signals, which can diffract around obstacles or penetrate through them to some extent, mmWave signals are highly directional and have limited diffraction capabilities. This reliance on LoS means that even small obstacles can have a significant impact on signal quality.

2 **Material-Specific Attenuation**: The degree of attenuation varies depending on the material of the obstructing object. For example:

   – **Brick walls**: Attenuation can range from 40 to 80 dB [6, 95], making it extremely challenging for mmWave signals to penetrate buildings constructed from such materials. This severe attenuation necessitates careful planning of mmWave networks in urban environments to avoid significant performance degradation.

   – **Human body**: Attenuation caused by the human body can range from 20 to 35 dB [48]. This means that even a person standing between the transmitter and receiver can significantly impact signal strength. This is particularly relevant in densely populated areas or indoor environments where people frequently move through the signal path.

   – **Foliage and Vegetation**: Trees and plants, particularly those with high water content, can cause considerable attenuation [60]. This is especially problematic in outdoor environments where vegetation is present. Seasonal changes and weather conditions can further exacerbate this issue, leading to variable signal quality.

Chapter 3

Object Tracking via Blockage

In this chapter, we track single or multiple objects by leveraging blockage phenomenon in mmWave communication [90, 94].

3.1 Introduction

Millimeter wave is widely used in radio astronomy, remote sensing, weather radar, security screening, clinical medicine, and so on. For telecommunications, millimeter wave is a promising technique for the next generation of cellular communication systems, due to its large frequency bandwidth. Another feature of millimeter wave is its narrow beam. For example, the beam of a 0.12m antenna is only 1.8°, which makes it capable to detect small targets more accurately.

However, a downside of millimeter wave is its strong blocking effect, namely an object in the propagation path may cause a severe channel attenuation (e.g., 10dB or even more). This is a critical problem in wireless communications, since a passing person, or even a leaf, may block your communications. A design of physical layer and directional MAC in 60 GHz Wireless Personal Area Networks (WPAN) is proposed to combat the blocking effect in millimeter wave communications [64]. Beam switching is proposed as an alternative solution to the blocking problem in WPANs in [8]. Besides, the propagation characteristics of blocking effect are thoroughly investigated

and summarized in [17] and [48]. Moreover, human body models, such as the multiple knife edge model [33], and cylinder model [39], have been proposed and studied in the aspect of movement.

Although the blocking effect may bring a significant damage to millimeter wave communications, it also brings potential benefits. Notice that the blocking damage corresponds to a blocking object. Hence successive severe performance degradations in multiple millimeter wave communication links imply the possibility of a passing object. Hence, the communication damages due to the blocking effect may facilitate the tracking of a moving object without the cost of any extra hardware (such as specifically designed tracking sensors). This is illustrated by Fig. 3.1, where in the movie *Entrapment* the movement of Zeta-Jones touches the visible beams (unless she avoids them deliberately), from which one may guess how her body moves if there are sufficient number of beams. Once the tracking or existence detection can be realized, it can be applied in many practical systems, such as human movement tracking, population estimation and law forensics (when there is no video camera). Therefore, the misfortune brought by the blocking effect in communications could be turned into a blessing event for the purpose of tracking and detection. Notice that a high-precision tracking approach is proposed based on millimeter waves [76]; however, it employs the reflection characteristics of millimeter waves in a similar manner to radar, which is completely different from the scheme proposed in this paper.

Existing approaches of multiple-object tracking are based on visualization. [14] introduces two intuitive and general metrics to track multiple people in real world. An efficient and robust visual object tracking algorithm based on the particle filter is proposed in [78]. Many other methods, such as spin-image [36], local image clustering [46] [47], K-shortest paths [13] are proposed to recognize multiple objects in 2-D or 3-D images. On the other hand, many millimeter wave tracking researches focus on automobile sensing, such as [26] and [32]. Meanwhile, [76] proposes a model to sense and track small size objects via multiple transceivers. However, all these existing

approaches require special devices. In a sharp contrast, the tracking approach in this paper leverages the byproduct of communication systems.

3.2 Experiments on Blocking Effect

3.2.1 Testbed

To study the characteristics of mmWave, we build a hardware testbed, shown in table 3.1.

Input

As shown in Fig. 3.2, Tektronix AFG3000C, an Arbitrary/Function Generator, generates a sine wave with 1MHz, 100mVpp and 50mV offset as the input of TX.

External Clock

To ensure that transmitted signal synchronizes with received signal, we connect both TX and RX to a 71.4285MHz external clock generated by Tektronix TSG4102A, an RF Vector Signal Generator, shown in Fig. 3.3.

Software

We install HMC6300/HMC6301 Graphical User Interface on two PCs and plug in the USB cable connected to the HMC6300 and HMC6301 motherboards assembly.

TX

In the motherboard, we connect **BB_IP** (connecting to the I positive baseband output) to the input signal, **EXT_CLOCK** to the external clock, USB to PC, **5V_SUPPLY** to a DC Power, and TX module to an antenna, shown in Fig. 3.4.

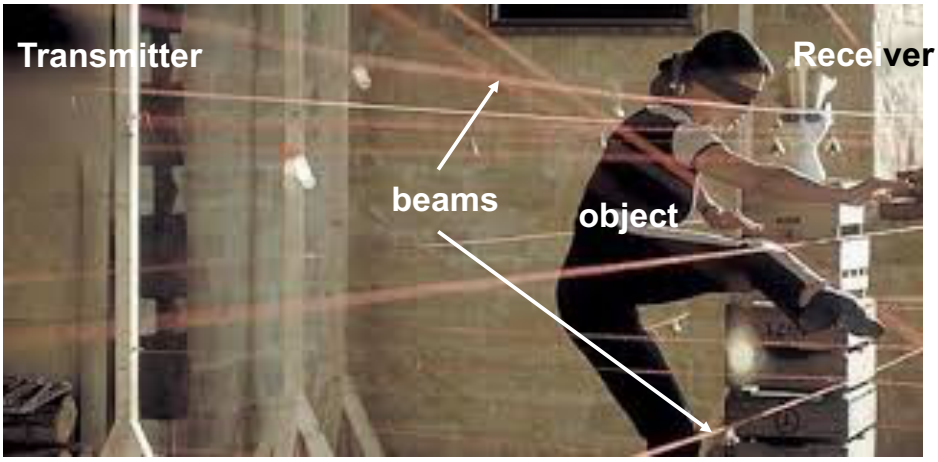


Figure 3.1: An illustration of the millimeter wave blocking based tracking, using the picture in *Entrapment*.

Table 3.1: Hardware Testbed Components

Component	Model
Transmitter	HMC6300 motherboard with the TX module
Receiver	HMC6301 motherboard with the RX module
Signal Source	Tektronix AFG3102C
External Clock	Tektronix TSG4102A
Antenna	QuinStar Pyramidal Horn
Oscilloscope	Tektronix DPO 70404C
Software	HMC6300/HMC6301 Graphical User Interface

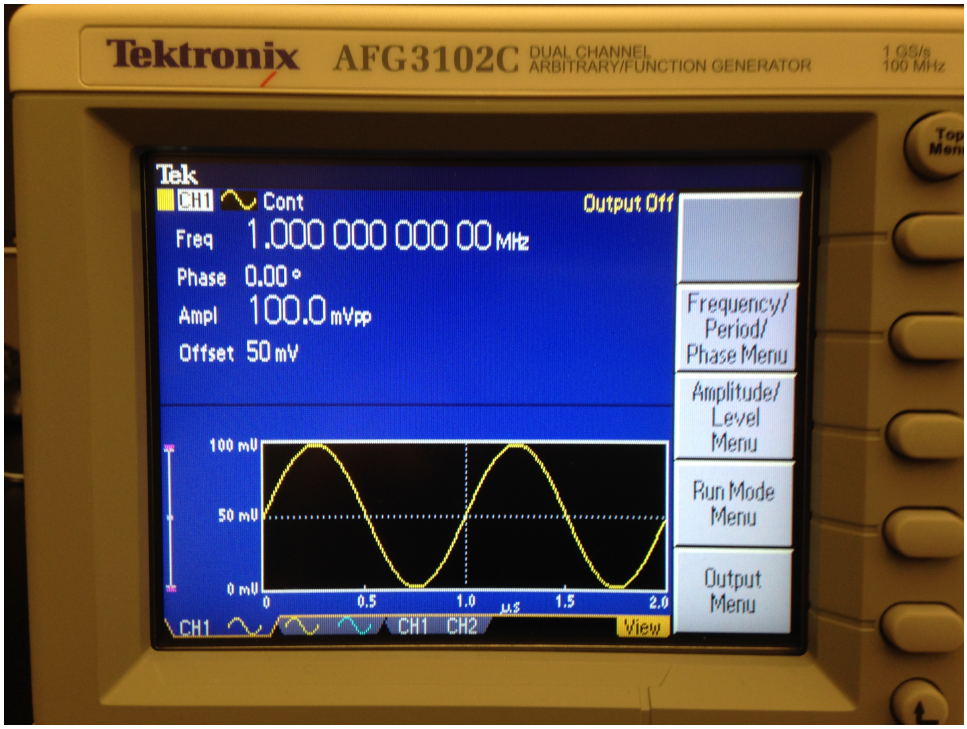


Figure 3.2: Input Signal.

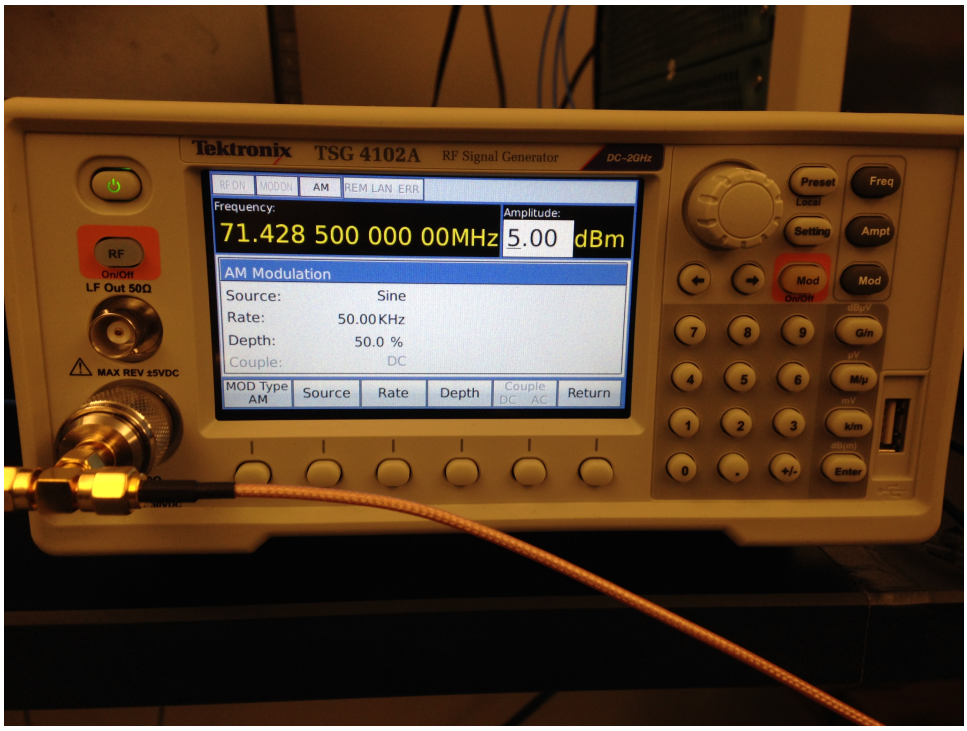


Figure 3.3: External Clock.

RX

To improve the resistance to electromagnetic interference, we use differential signaling in RX. Similar to TX, we connect **VOUT_IP**, **VOUT_IM**, **VOUT_QP** to oscilloscope channel 1 and 2, **EXT_CLOCK** to the external clock, USB to PC, **5V_SUPPLY** to a DC Power, and RX module to an antenna, shown in Fig. 3.5.

Remark 1. ***VOUT_QM*** *shares the same ground with* ***VOUT_IM****, so we leave it unconnected.*

3.2.2 Procedure

The experimental setup is given in Fig. 3.6. The whole process is as follows:

1. The signal source generates a 100MHz sinusoidal baseband signal, and feeds it to the transmitter,
2. The transmitter upshifts the input signal to 60GHz and emits via the horn antenna.
3. The 60GHz signal is blocked somewhere on the line of sight (LoS), or not, and received via a horn antenna,
4. The receiver downshifts the received signal to the base band, and displays the baseband signal on the oscilloscope.

Sufficiently many samples are stored in the buffer for further offline analysis. Fig. 3.7 is a live picture of the experiment, where the author passed the beam of the 60GHz transceiver testbed.

3.2.3 Scenarios and Results

Different scenarios have been tested using the above devices and setup. Notice that some results verified existing reports on the blocking effect of millimeter wave, while other results provide useful information for the purpose of tracking based blocking.

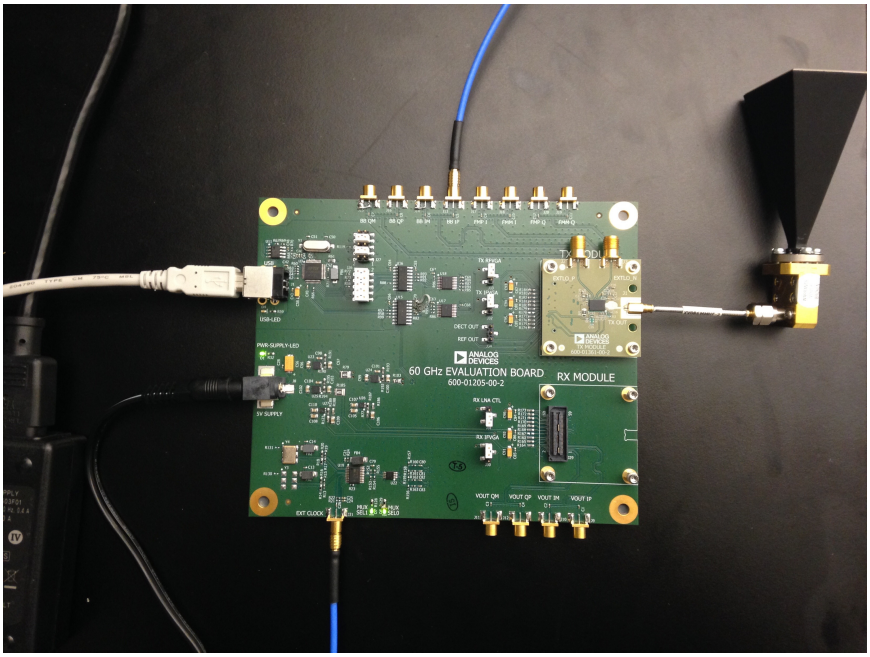


Figure 3.4: HMC6300 Motherboard/TXModule Assembly with USB, DC Power, Antenna, External Clock and I/Q Cables Installed.

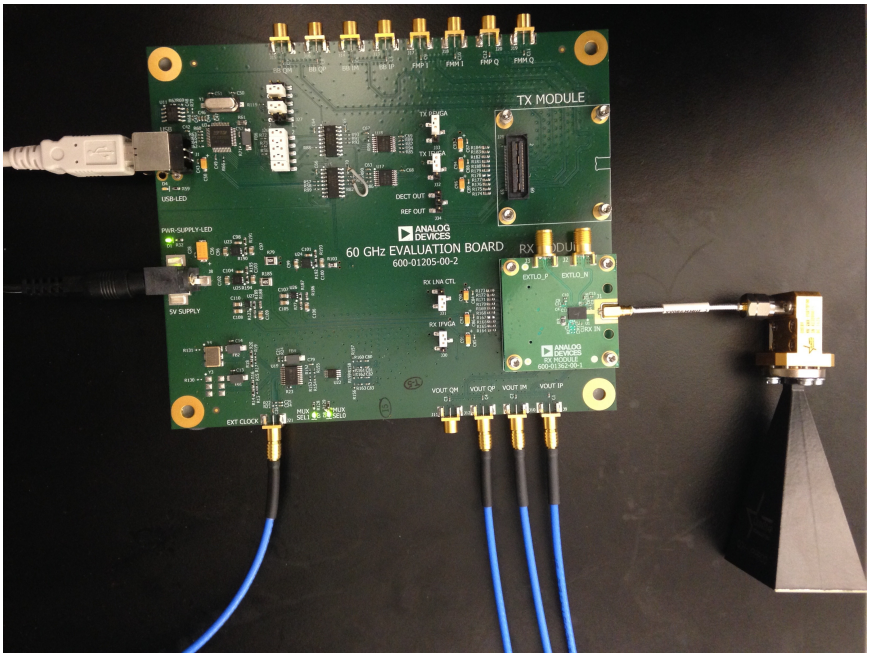


Figure 3.5: HMC6301 Motherboard/RXModule Assembly with USB, DC Power, Antenna, External Clock and I/Q Cables Installed.

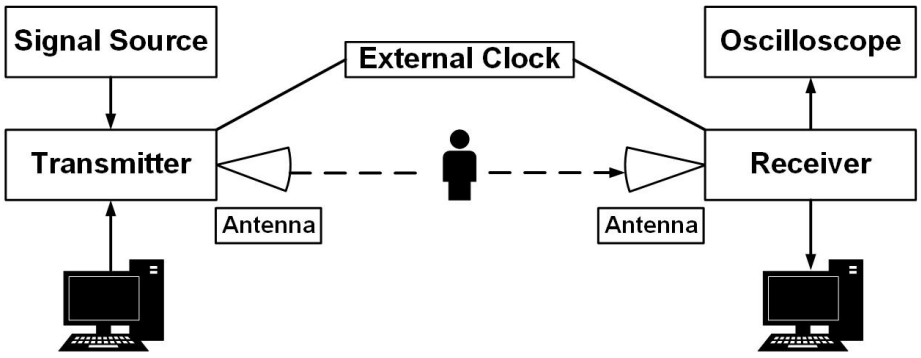


Figure 3.6: The experiment setup

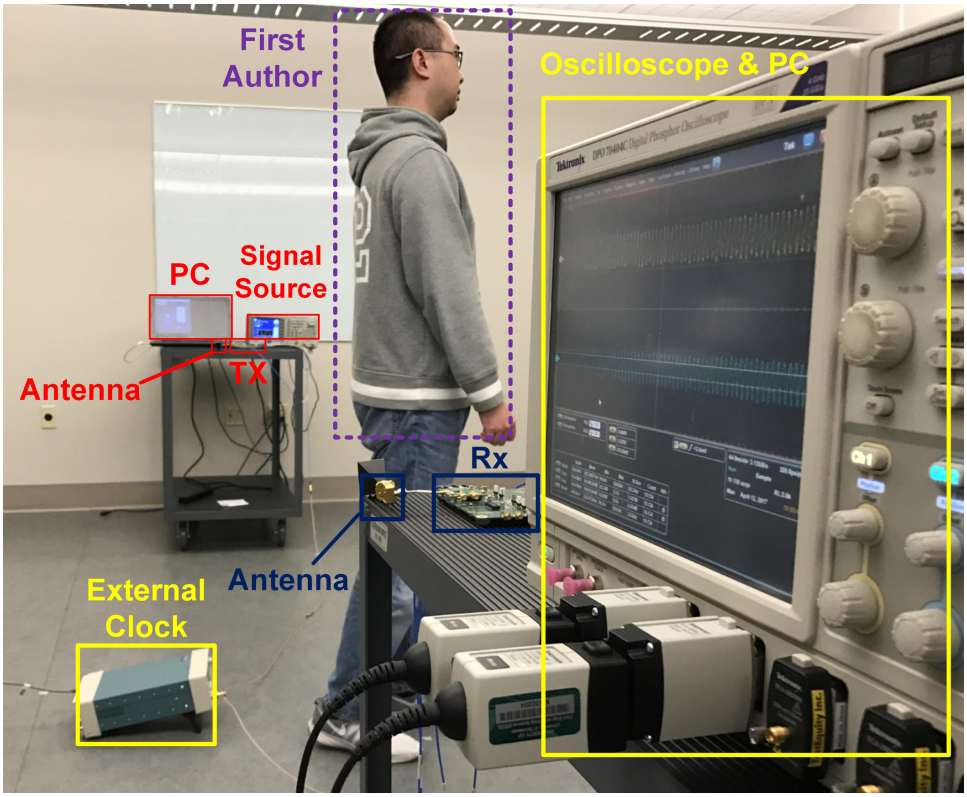


Figure 3.7: Live picture of the experiment.

Reflection

The distance between TX and RX is set to 5 meters. The centers of TX and RX antennas are in a horizontal line. We aim both horn antennas at a 30° degree to the ground to make sure that only reflection paths, not LoS, are available. The measurements show that the attenuation of the ground reflection is about 25dB in the experiment setup. Hence, we can focus on the LoS and ignore the reflection paths.

Static Blocking Scenario

In this case, the distance between TX and RX is set to 5 meters. The axes of TX and RX antennas are along the LoS. A person stands right on the LoS and blocks the signal in the center. As the person stands at different locations along the LoS, we record the received signal and calculate the corresponding signal-to-noise ratio (SNR). Then the person steps half pace away from LoS in the vertical direction and partially blocks the signal. Repeating the process, we obtain the relationship between the SNR and the distance to the TX in Fig. 3.8. We observe that there is a significant SNR degradation when the LoS is blocked, regardless of centered or partial one.

Dynamic Blockage Scenario

In this scenario, the person walks through the LoS in the vertical direction. The sampling rate is adjusted to 2.5MS/s, and the recording length is set to 12.5M (the maximum length), such that we can record a time duration of around 5 seconds. The frequency of the baseband signal was reduced to 100KHz in case of sampling distortion. Fig. 3.9 shows the changing of signal amplitude with time, where the distance to TX is 0.5m. Meanwhile, the relationship between the SNR and the distance to the TX is plotted in Fig. 3.10. The results are similar. We can conclude that it is easy to detect a person passing through the LoS instantaneously, since the SNR varies significantly in the process.

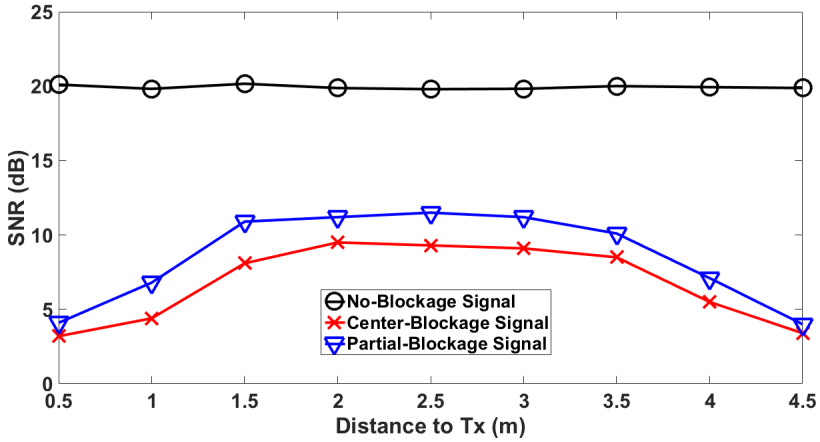


Figure 3.8: SNR varies with distance in static blockage scenario.

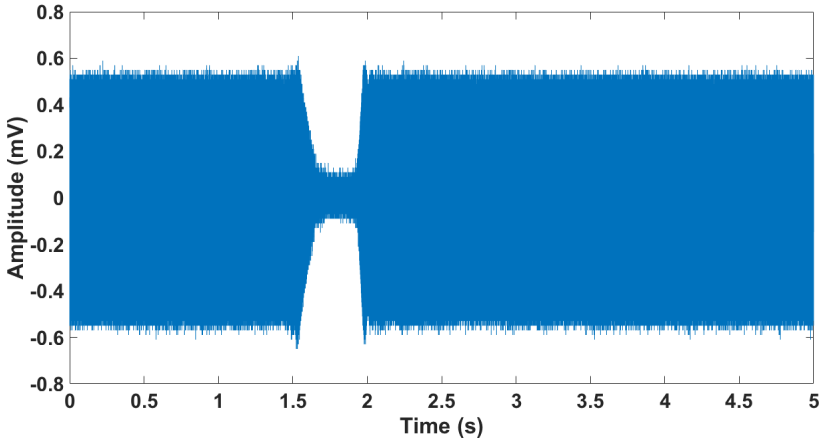


Figure 3.9: The change of amplitude when a person passes the LoS.

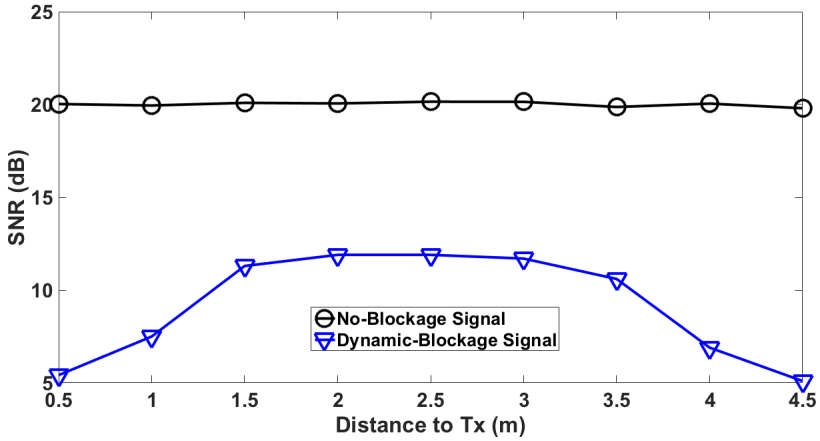


Figure 3.10: SNR varies with distance in dynamic blockage scenario.

According to our experiment results, we can draw the following conclusions related to the tracking algorithm proposed later:

- Millimeter wave has an optical-like propagation. The blockage effect is significant, while the reflection is too weak to affect the SNR drop.
- The variance of SNR is significant. The SNR varies substantially in different experiments even under the same setup. Unfortunately, though the SNR varies with different blocking locations (the distance to the TX), it is not reliable to determine the location of the blocking object on the LoS. The only available information is the occurrence of blocking (in terms of significant SNR drop) and the corresponding time.

3.3 Single Object Tracking

In this section, we propose two criteria for the tracking algorithm based on the blocking effect of millimeter wave.

3.3.1 Problem Formulation

As shown in Fig. 3.11, we assume that a pedestrian walks passing $N+1$ millimeter wave communication links $\{(TX_0, RX_0), (TX_1, RX_1), ..., (TX_N, RX_N)\}$ at times $\{t_0, t_1, ..., t_N\}$. The black curve represents the real trajectory. Our goal is to estimate the pedestrian's trajectory by locating its intersecting coordinates on each communication link, denoted by a 2-tuple $\mathbf{z}_n$ for link n. The trajectory between two blocking events is approximated by a line segment for simplicity. Due to the uncertainty of the trajectory, optimization criteria with reasonable assumptions on the trajectory are needed.

3.3.2 Shortest Path Criterion

The first criterion is based on the following assumption:

Initialize the distance-to-go array $D(N, 1:M) = 0$.
for $t = N-1, ..., 0$ **do**
  for $m = 1, ..., M$ **do**
    Set $D(t, m) = \min_{m'} \|\mathbf{z}_{t,m} - \mathbf{z}_{t+1,m'}\| + D(t+1, m')$.
    Set $H(t, m) = m'$.
  end for
end for
Choose $m_0^* = \arg\min_m D(0, m)$. Randomly choose one if there is a tie.
for $t = 1, ..., N$ **do**
  Set $m_t^* = H(t-1, m_{t-1}^*)$.
end for
Output $\left\{\mathbf{z}_{0,m_0^*}, ..., \mathbf{z}_{N,m_N^*}\right\}$.

Algorithm 1: Dynamic Programming for the Shortest Trajectory Optimization

Hypothesis 1. *The pedestrian prefers the shortest trajectory.*

Then, the tracking algorithm is formulated as

$$\begin{aligned} &\min_{\mathbf{z}_0,\ldots,\mathbf{z}_N} \sum_{n=0}^{N-1} \|\mathbf{z}_{n+1} - \mathbf{z}_n\| \\ s.t. \quad &\mathbf{z}_n \text{ is on the LoS of } TX_n \text{ and } RX_n, \forall n = 0, ...N. \end{aligned} \tag{3.1}$$

The optimization problem in (3.1) can be readily solved by using the dynamic programming (DP), which simplifies the problem by breaking it down into simpler sub-problems in a recursive manner. The key challenge is that each location $\mathbf{z}_n$ is continuous; thus one has infinitely many choices for each stage. Therefore, we discretize the LoS line segment by uniformly choosing M points on the LoS between each TX and RX, such that there are M^{N+1} possible trajectories. The corresponding coordinates are denoted by $\{\mathbf{z}_{nm}\}_{n=0,...,N,m=1,...,M}$. Then we obtain the shortest trajectory by using DP with discrete system states (the locations on the LoS), which is very similar to the Viterbi decoding algorithm. The algorithm is summarized in Procedure 1. By using DP algorithm, we have a series of coordinates $\{\mathbf{z}_0, ..., \mathbf{z}_N\} = \{(x_0, y_0), (x_1, y_1), ..., (x_N, y_N)\}$, as shown in Fig. 3.11.

3.3.3 Minimum Velocity Variance Criterion

A shortcoming of the shortest path is that it may underestimate the path between two successive millimeter communication links, since it does not utilize the timing information. To utilize the timing information, we can exploit the velocity information by proposing the following hypothesis:

Hypothesis 2. *The pedestrian prefers a constant speed, such that the variance of speed is minimal.*

The resulting difference between the two criteria is illustrated in Fig. 3.12, where three links, together with the recorded timing of blocking events, are displayed. If we consider only the shortest path, we may choose the upper trajectory candidate. However, this means that the object almost triples its velocity after passing link 2, which is less reasonable. As will be seen, the minimum velocity variance criterion can yield a better performance at the cost of more computational cost.

Then, using the minimum velocity variance criterion, the tracking algorithm is formulated as

$$\min_{\mathbf{z}_0,...,\mathbf{z}_N} Var(v_0, v_1, ..., v_{N-1}) \tag{3.2}$$

$$s.t. \quad \mathbf{z}_n \text{ is on the LoS of } TX_n \text{ and } RX_n, n = 0, ...N$$

$$v_n = \frac{\|\mathbf{z}_{n+1} - \mathbf{z}_n\|}{t_{n+1} - t_n}, n = 0, ..., N-1 \tag{3.3}$$

Unfortunately, there is no algorithm like DP to obtain the optimal solution to (3.2). Hence, we use the gradient descent (GD) approach to reduce the velocity variance incrementally. See Fig. 3.11. Let $\{(x_0, y_0), (x_1, y_1), ..., (x_N, y_N)\}$ be initial estimated coordinates, which can be obtained from the above shortest path approach and simply the middle point of each LoS link. Since the coordinates of all (TX, RX) are known, we can write the vertical coordinate as

$$y_n = a_n x_n + b_n, \qquad n = 0, ..., N. \tag{3.4}$$

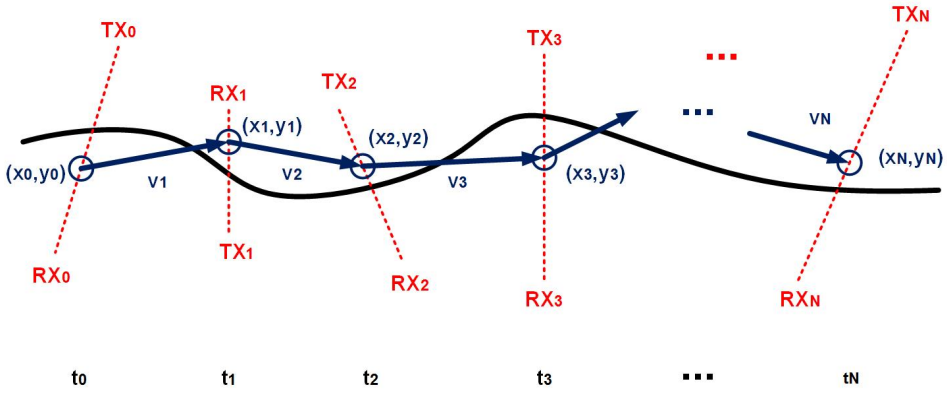


Figure 3.11: Coordinates and speeds in estimated path.

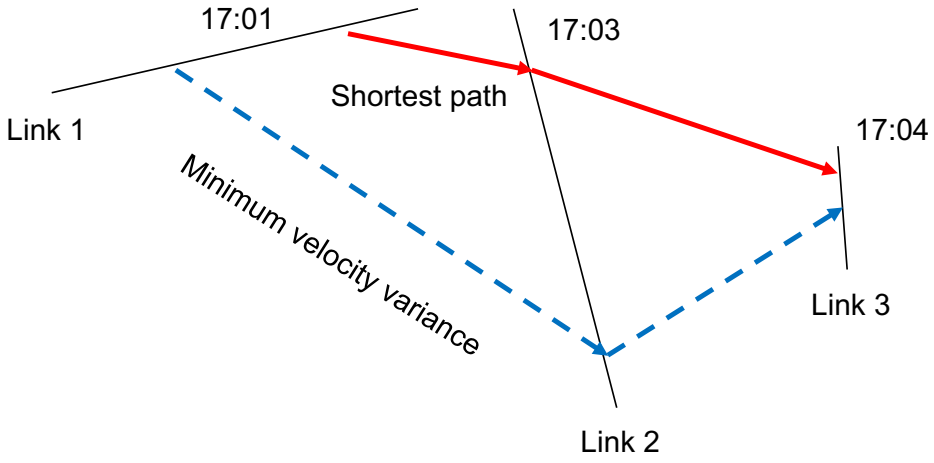


Figure 3.12: Comparison between the two criteria.

1: Initialize the coefficient γ.
2: Obtain $(a_0, b_0), (a_1, b_1), ..., (a_N, b_N)$ from the coordinates of communication links.
3: Initialize $(x_0, y_0), (x_1, y_1), ..., (x_N, y_N)$ (e.g., choosing middle points of all communication links.)
4: **while** Not converged **do**
5: Calculate $\nabla Var(x)$ by (3.5).
6: **for** $n = 0, ..., N$ **do**
7: Update $x_n = x_n - \gamma \frac{\partial Var}{\partial x_n}$.
8: Update the velocity v_n.
9: **end for**
10: **end while**

Algorithm 2: Gradient Descent Algorithm

where a_n and b_n are the slope and offset of the LoS n.

Using straightforward calculus, the gradient of velocity variance, ∇Var, is given by

$$\begin{aligned}
\frac{\partial Var}{\partial x_n} = & \frac{2a_n(a_n x_n + b_n - a_{n-1}x_{n-1} - b_{n-1}) + 2(x_n - x_{n-1})}{n(t_n - t_{n-1})^2} \\
- & \frac{(2a_n(a_n x_n + b_n - a_{n-1}x_{n-1} - b_{n-1}) + 2(x_n - x_{n-1}))\left(\sum_{i=1}^{N} v_i\right)}{n^2(t_n - t_{n-1})\sqrt{(a_n x_n + b_n - a_{n-1}x_{n-1} - b_{n-1})^2 + (x_n - x_{n-1})^2}} \\
- & \frac{2a_n(a_{n+1}x_{n+1} + b_{n+1} - a_n x_n - b_n) + 2(x_{n+1} - x_n)}{n(t_{n+1} - t_n)^2} \\
+ & \frac{(2a_n(a_{n+1}x_{n+1} + b_{n+1} - a_n x_n - b_n) + 2(x_{n+1} - x_n))\left(\sum_{i=1}^{N} v_i\right)}{n^2(t_{n+1} - t_n)\sqrt{(a_{n+1}x_{n+1} + b_{n+1} - a_n x_n - b_n)^2 + (x_{n+1} - x_n)^2}}, \\
& n = 0, ..., N.
\end{aligned} \tag{3.5}$$

Then, the detailed algorithm of the minimum velocity variance criterion is summarized in Procedure 2.

3.3.4 Performance Analysis

In this section, we evaluate the performance of the tracking algorithm analytically. We consider two scenarios that simplify the analysis.

Analysis with Simplified Trajectory

To simplify the problem, we use the following simplified model of trajectory:

- We assume that the trajectory consists of a series of straight lines (the object moves straight) and circular arcs (the object makes a turn).
- We assume that the intersection points of the trajectory and the LoS lines are perfectly determined.
- We assume that there is no tracking error in the straight line portion, since a straight line can be determined by merely two points. Hence, we focus on the arc part.

The above assumptions simplify the analysis and can serve as a bound for the performance. The validity can be visually demonstrated by the true pedestrian trajectories such as Fig. 3.16.

An illustration is given in Fig. 3.13. We notice that the trajectory during the arc part is approximated by the chords between the intersection points. Since we focus on only the arc part, the trajectory estimation error is essentially determined by the error between the arc and the chords.

Given the simplified model of trajectory, the performance bound is given in the following theorem.

Theorem 3.1. *Assume that the above simplified model of trajectory holds and the assumptions on the tracking algorithm are valid. Consider an arc trajectory of angle* $\phi \leq \pi$ *and radius* r*, intersecting* N *communication links. Define* $e_{\max}$ *as the maximum*

gap between the arc and the chords determined by the intersection points (as illustrated in Fig. 3.14). Then, we have an upper bound

$$E[e_{\max}] \leq r\left(1-\cos\left(\frac{\phi}{2(N+1)}H_{N-1,1}\right)\right), \tag{3.6}$$

and a lower bound

$$\begin{aligned} E[e_{\max}] \;&\geq\; r\left(1-\cos\left(\frac{\phi}{2(N+1)}H_{N-1,1}\right)\right) \\ &-\; \frac{r}{4}\int\int (x-y)^2 h(x)h(y)dxdy, \end{aligned} \tag{3.7}$$

where $H_{N-1,1}=\sum_{k=1}^{N-1}\frac{1}{k}$ *and* h *is the pdf of* $e_{\max}$ *given by*

$$h(x)=\frac{1}{\phi}\sum_{i=1}^{\lfloor\frac{1}{x}\rfloor} i(n-1)\begin{pmatrix} n \\ i \end{pmatrix}\left(1-\frac{ix}{\phi}\right)^{n-2}. \tag{3.8}$$

Proof. The N intersection points are dropped on the unit circular arc. Denote the angles of the intersection points by ordered $\theta_1 \leq \theta_2 \leq ... \leq \theta_N$, and the angle differences between every two neighboring points by $\{d_1, d_2, ..., d_{N-1}\}$. For simplicity, we normalize the angles to $\theta_1 = 0$ and $\theta_N = 1$. According to (6.4.2) in [18], the probability density function of d_i is given by

$$f(d_1, ..., d_{N-1}) = (N-2)! \tag{3.9}$$

By using the conclusion in [59], the expectation of maximum distance is

$$E[d_{max}(N)] = \frac{1}{N+1}H_{N-1,1}, \tag{3.10}$$

where $H_{N,1}=\sum_{k=1}^{N}\frac{1}{k}$ is the generalized harmonic number.

Normalizing back to the angle range $[0, \phi]$, we have

$$E[d_{max}(N)] = \frac{\phi}{N+1} H_{N-1,1}, \tag{3.11}$$

For a single d, the corresponding error e between the arc and the chord is illustrated in Fig. 3.14. It is easy to verify that

$$e = r\left(1 - \cos\frac{\theta}{2}\right). \tag{3.12}$$

Hence, the expectation of the maximum error is given by

$$E[e_{\max}] = r\left(1 - E\left[\cos\frac{d_{\max}}{2}\right]\right). \tag{3.13}$$

Notice that the pdf of $e_{\max}$ can be obtained using the formula (6.4.4) in [18].

Since the function cos is a concave function in $[0, \pi/2]$, we have

$$\begin{aligned} E[e_{\max}] &\leq r\left(1 - \cos E\left[\frac{d_{\max}}{2}\right]\right) \\ &= r\left(1 - \cos\left(\frac{\phi}{2(N+1)} H_{N-1,1}\right)\right) \end{aligned} \tag{3.14}$$

according to the Jensen's inequality.

By applying the Hölder's defect formula (Problem 6.5 in [65]), we have

$$\begin{aligned} E\left[\cos\frac{d_{\max}}{2}\right] &\leq \cos E\left[\frac{d_{\max}}{2}\right] \\ &+ \frac{1}{4}\int\int (x-y)^2 h(x)h(y)dxdy. \end{aligned} \tag{3.15}$$

This concludes the proof. □

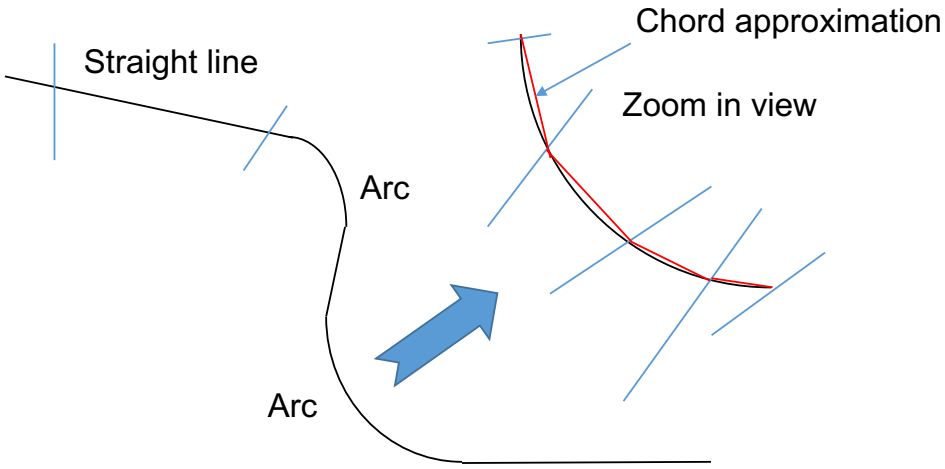


Figure 3.13: An illustration of the simplified model of trajectory.

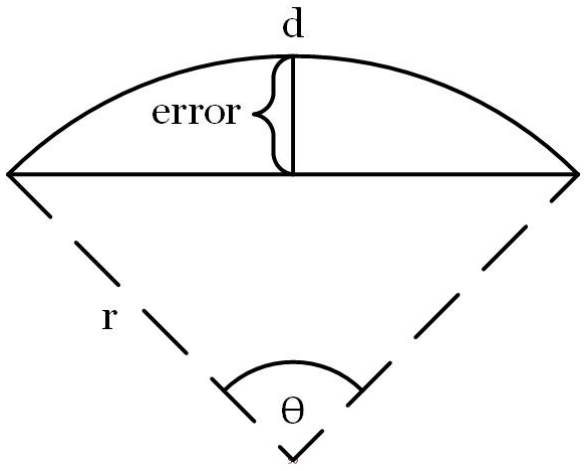


Figure 3.14: Illustration of error between the arc and chord

Asymptotic Analysis of Dense Networks

Now we consider a network in a compact region and study the tracking error when the node density tends to infinity. We assume that the transmitters are uniformly and independently distributed in a compact region with density ρ (namely the number of transmitters in a unit area), as a 2-dimensional Poisson point process. The cumulative distribution function (cdf) of the transmitter-receiver distance is given by g. Moreover, we assume that the positions of the receivers are mutually independent. The worst case tracking error, namely the maximum distance between the true and estimated positions, is denoted by e_w. Then, the following theorem shows that e_w tends to zero in probability as $\rho \to \infty$ given certain conditions.

Theorem 3.2. *Suppose that the trajectory is smooth and the curvature is bounded. We also assume that $g(x) > 0$ for any $x > 0$. Then, for all $\epsilon > 0$, we have*

$$\lim_{\rho \to \infty} P(e_w \geq \epsilon) = 0, \tag{3.16}$$

namely e_w converges to 0 in probability.

Proof. We assume that the trajectory length is $L < \infty$. Fix an $\epsilon > 0$, we cover the trajectory with circles of radius ϵ centered at points on the trajectory with indices $i = 1, ..., K$, where $K = \left\lceil \frac{L}{\epsilon} \right\rceil$. We fix one end of the trajectory as the starting point. Then curve length between the starting point and center i is given by $i\epsilon$. This is illustrated in Fig. 3.15 (a).

Consider center/circle i. The probability that k transmitters fall in the circle with radius $\frac{\epsilon}{2}$ and centered at center i is given by

$$q_k(\epsilon) = e^{-\frac{1}{4}\rho\pi\epsilon^2} \frac{(\rho\pi\epsilon^2)^k}{4^k k!}, \qquad k = 0, 1, ... \tag{3.17}$$

due to the Poisson process assumption [80]. Then, for each transmitter falling in the $\frac{\epsilon}{2}$-circle, the probability that its receiver falls in the other side of the trajectory but

still within the ϵ-circle is lower bounded by

$$Q(\epsilon) \geq g(\epsilon)\eta, \tag{3.18}$$

where η is the ratio between the shaded area and the circle area in Fig. 3.15 (b). Hence, the probability that we can find at least one communication link whose both transmitter and receiver are within the ϵ-circle is bounded by

$$\Theta(\epsilon) \geq \sum_{k=1}^{\infty} q_k(1-(1-Q(\epsilon))^k). \tag{3.19}$$

Obviously, if we can find a communication link within each ϵ-circle, the tracking error e_w is upper bounded by $A\epsilon$, where A is a constant determined by the bounded curvature. The failure probability is upper bounded by

$$P(e_w \geq A\epsilon) \leq (1-\Theta(\epsilon))^K \to 0, \tag{3.20}$$

as $\rho \to \infty$, since it is easy to verify that $\Theta(\epsilon) \to 1$ as $\rho \to \infty$. This concludes the proof.

□

3.3.5 Numerical Simulations

In this section, we present numerical simulations of the proposed schemes using real trajectories. We use GPS to record pedestrian walking trajectory. The accuracy of GPS data is about 1 meter, and the minimal time interval is 1 second, which are of sufficient precision for most applications. The millimeter wave communication links are randomly dropped into the region. The distance of communication link is uniformly distributed between 15m and 70m. Then, we show the DP and GD estimations together with the actual trajectory in Fig. 3.16. We can observe that the GD estimation is much closer to the actual trajectory than DP.

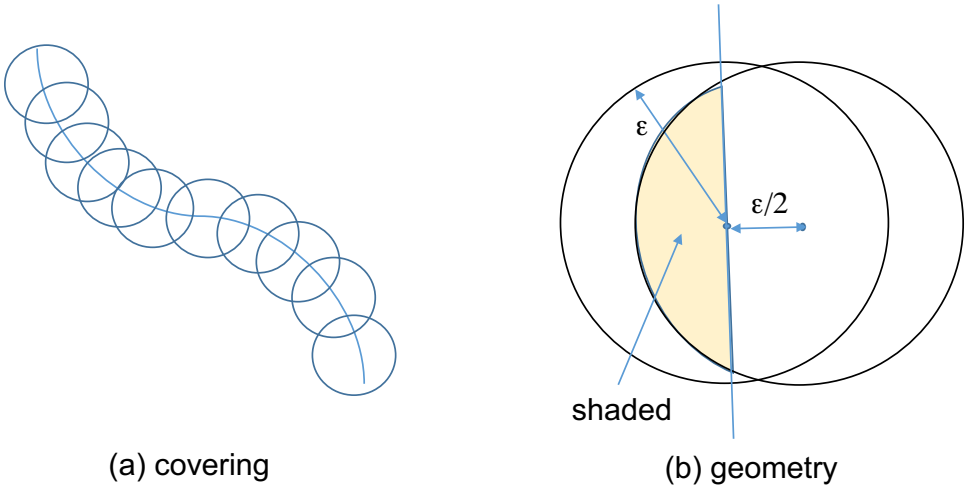


Figure 3.15: Illustration of the covering and geometry in the proof of Theorem 3.2

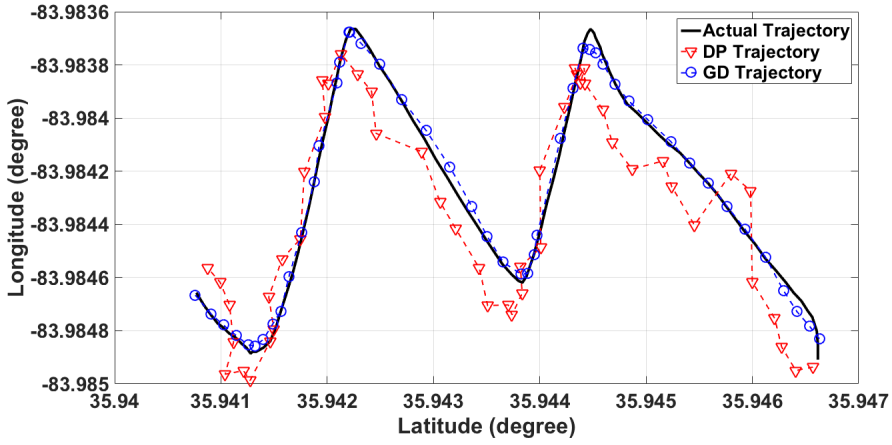


Figure 3.16: DP estimation, GD estimation and actual trajectories

Then we calculate the corresponding average and maximum estimation errors, which are the average and maximum distances between the estimated and actual coordinates, respectively, measured in meters. The result, as a function of the communication link density, is shown in Fig. 3.17. We find that the average and maximum estimation errors of both algorithms decreas as the communication link density increases. We observe that the estimation error in GD is much smaller than that in DP.

On the contrary, in the same situation, the time cost of GD is about five times higher than DP, as shown in Fig. 3.18. As the density increases, the calculation of GD will be much slower.

Furthermore, we change the average length of the communication link. As expected, the estimation error and average length of communication link have the same trend in Fig. 3.19. However, when we consider the relative estimation error rate, which is the ratio between the estimation error and the length of communication link, the trend is opposite, as shown in Fig. 3.20. It means that the length increment of communication link will relatively lessen the estimation error.

Finally, we fix the communication link density and average length, calculate the estimation errors of 20 different GPS based trajectories in Fig. 3.21. We find that the estimation error varies substantially in different trajectories under different circumstances. We still observe that the GD scheme outperforms DP unanimously. Meanwhile, Fig.3.21 is plotted in the descending order of average curvature, which means that the more curvy the trajectory is, the more accurately we can estimate it.

3.3.6 Conclusion

We have carried out experiments to assess the blocking effect in millimeter wave. The results have shown that a passing object can be easily detected via the blocking of communication, whereas it is infeasible to determine the precise location of object. Two criteria, namely the shortest path and minimum velocity variance, have

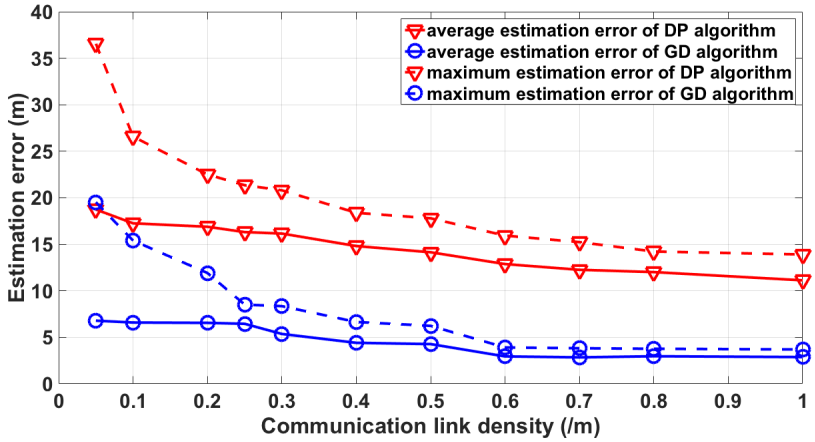


Figure 3.17: Estimation error in terms of communication link density

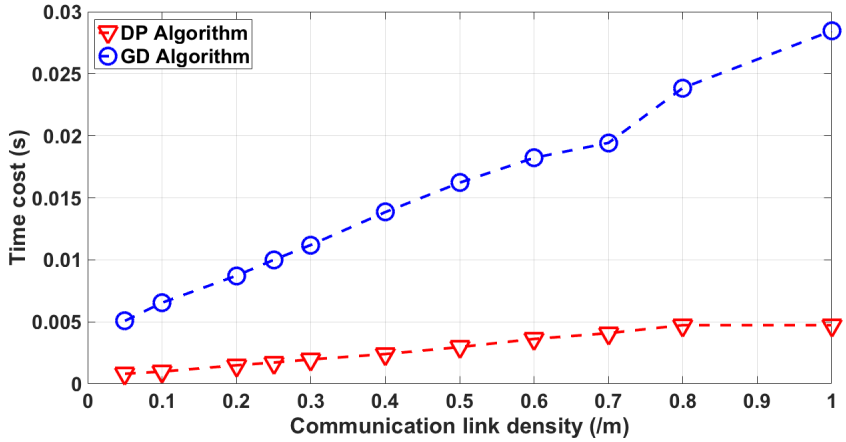


Figure 3.18: Computation cost in terms of communication link density

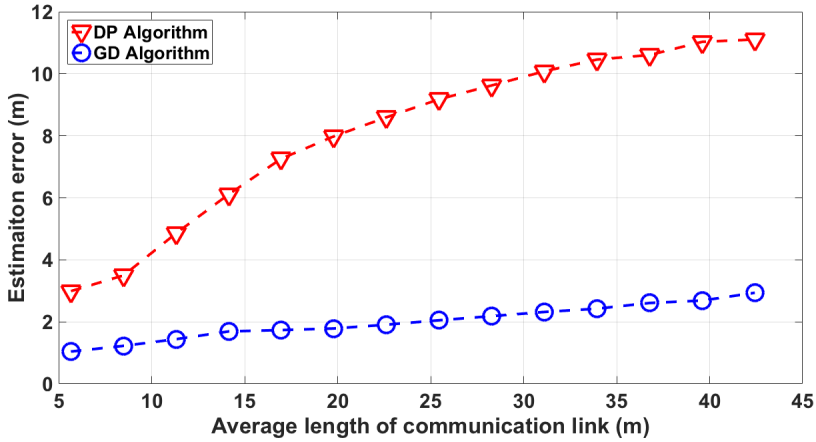


Figure 3.19: Estimation error in terms of average communication link length

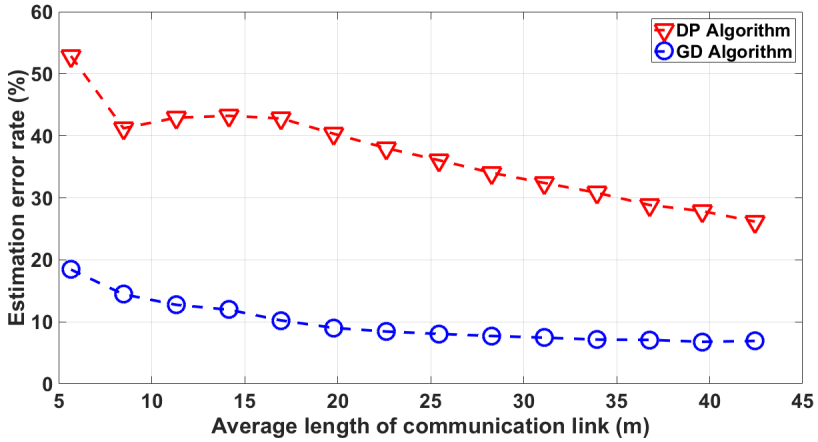


Figure 3.20: Relative estimation error in terms of average communication link length

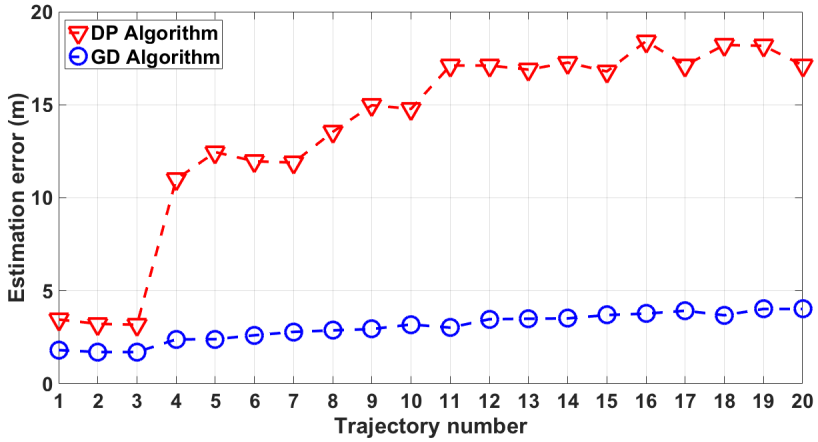


Figure 3.21: Histogram of estimation errors

been proposed to design the tracking algorithm based on the blocking effect. The performance of tracking has been analyzed for both simplified model and asymptotic case analytically. Then, the estimation of trajectory has been compared with GPS based real trajectory, which shows the validity of the proposed tracking algorithms.

3.4 Multiple Objects Tracking

In this section, we propose a long term tracking algorithm for multiple moving objects, based on the blockage records of multiple millimeter wave communication links. We will first formulate the problem and then convert it to an intuitive geometric problem. Finally we carry out a theoretical analysis for the proposed algorithm.

3.4.1 Problem Formulation

Assume that there are M objects, each of which passes through N millimeter wave communication links in the same order. We assume that M is known. In practice, M can be obtained from the number of blockage events on each communication link. We index different objects using the orders of the starting time. Each communication link consists of a transmitter (T) and a receiver (R), whose corresponding coordinates are known in advance and are denoted by $\{(T_{1_x}, T_{1_y}), (R_{1_x}, R_{1_y})\}$, ...,$\{(T_{N_x}, T_{N_y}), (R_{N_x}, R_{N_y})\}$. The time of the j-th blockage events on communication link i is denoted by T_{ij}. Our goal is to estimate the trajectory of each moving object using all these available information. Meanwhile, we need to determine the identification of the corresponding moving object for each blockage time. We focus on the second problem, namely the object recognition. Once the identities of objects are recognized, we can obtain the series of blockage events for each individual object. Then, the problem of multiple objects is converted to that of a single object, and thus can be solved by using the single-object algorithm in [93]. This is illustrated in Fig. 3.22.

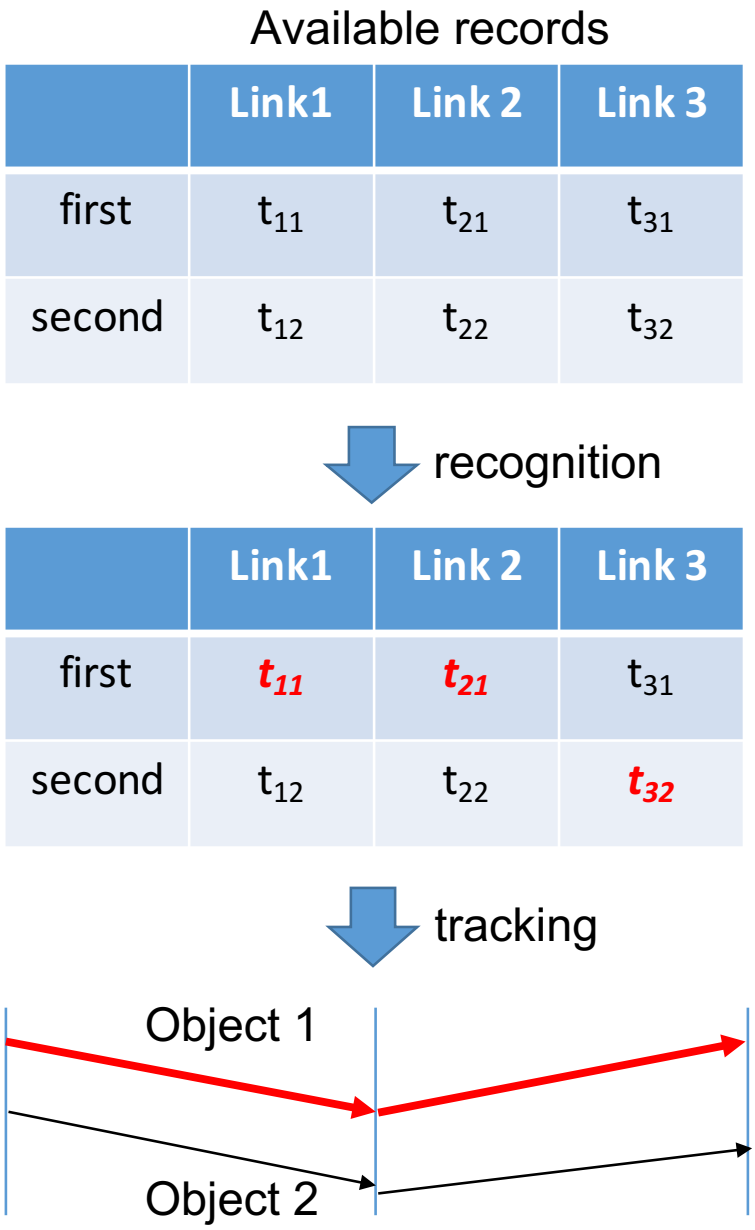


Figure 3.22: The two stages of trajectory tracking for multiple objects.

3.4.2 Geometric Heuristics

For the above problem formulation, we can cast it in geometrical heuristics illustrated in Fig. 3.23, based on which we propose an efficient algorithm for the object recognition. We consider the plane whose horizontal axis (called the d-axis) is the distance covered by the moving object and whose vertical axis is the time (called the t-axis). A blockage event can be represented by a line segment parallel to the d-axis, whose projection to the t-axis corresponds to the time of the blockage event, and whose projection to the d-axis corresponds to the possible distance covered by the object (starting from the first communication link). We call these parallel line segments windows. Each window has a time stamp and an index of the communication link. The uncertainty of the distance is due to the uncertainty of the intersection points of the object trajectory with the LOS lines of the communication links. We denote by $(d_{i,\min}, d_{i,\max})$ the range on the i-th communication link on the d-axis. They can be obtained from the locations of the transmitters and receivers. A two-object scenario is illustrated in Fig. 3.23.

3.4.3 Recognition Algorithm

Based on the geometric image, we develop an efficient algorithm for distinguishing different objects. First, we consider the uncertainty in the moving speed of each object. We assume that the average speed of each object is within an interval $[v_{m,\min}, v_{m\,\max}]$, $m = 1, ..., M$. Then, the possible time-distance trajectory of an object is a cone, whose boundaries are determined by the bounds of speed, as illustrated in Fig. 3.24.

Notice that the true trajectory of an object needs to intersect N windows of different communication link indices in the d-t plane. Hence, the corresponding cone also intersects N windows. However, the bounds of average speed $(v_{m,\min}, v_{m,\max})$ are unknown in advance. A reasonable assumption is that the speed variation is upper bounded by a constant δv, namely $v_{m,\max} - v_{m,\min} \leq \delta v$. Geometrically speaking,

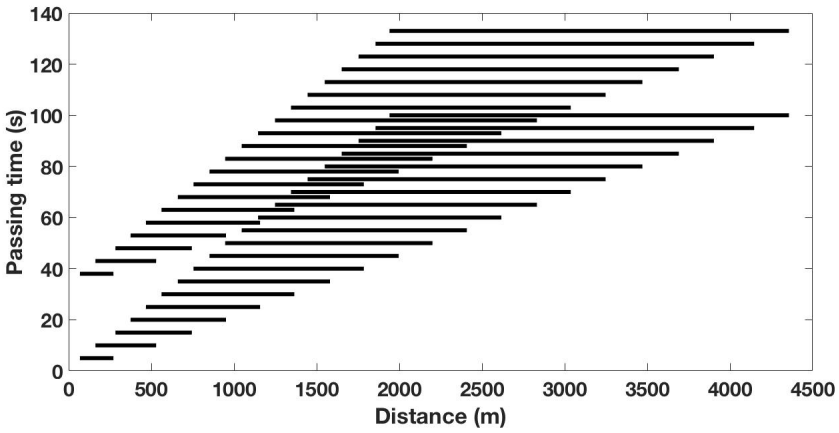


Figure 3.23: Distance range in terms of passing time in two objects scenario.

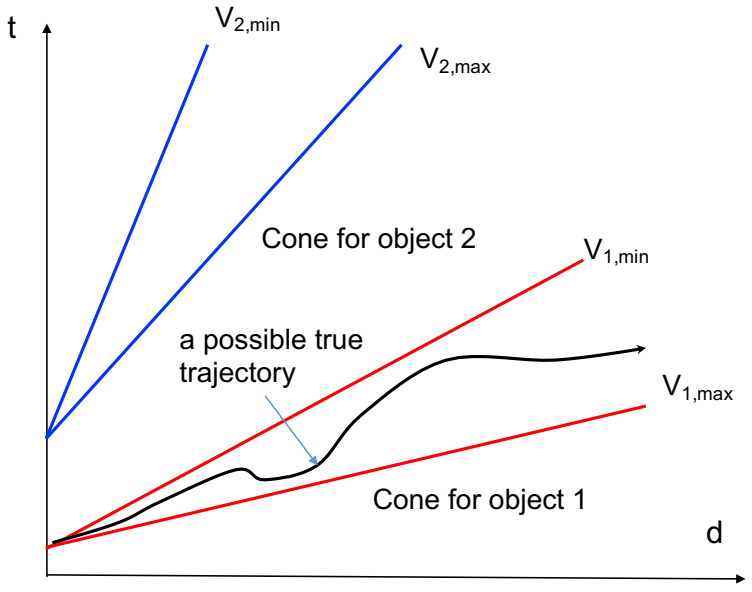


Figure 3.24: Cones of different moving objects.

the angle of each cone is bounded by δv. Motivated by the cone representation of the object trajectory range, for object m, we can consider a cone anchored at point $(0, T_{1m})$ with angle δv. We rotate the cone around the anchor point, with a step $\delta\theta$. Once the cone intersects N windows of different communication link indices, we claim that a reasonable trajectory is found and ascribe all the corresponding blockage events to object m. The detailed algorithm is summarized in Procedure 3.

1: **for** Object $m = 1, .., M$ **do**
2: **for** $k = 1 : \lfloor \frac{\pi}{2\delta\theta} \rfloor$ **do**
3: Set the center angle $\theta = k\delta\theta$.
4: Find the anchor point $(0, T_{1m})$ and the boundaries according to δv.
5: Find the windows intersecting the cone.
6: **if** There are N successive intersecting windows **then**
7: Ascribe the corresponding blockage events to object m.
8: Break the loop.
9: **end if**
10: **end for**
11: **end for**

Algorithm 3: Multiple Objects Recognition

3.4.4 Performance Analysis

Now, we analyze the performance of the proposed algorithm using the geometric intuition. For simplicity, we focus on the case of two moving objects. It is obvious that the two objects are confused only in the overlap region of the corresponding cones, as illustrated in Fig. 3.23. Denote the areas of object 1, object 2 and overlap region by S_1, S_2 and $S_{overlap}$, respectively. The recognition rate of object 1 is then given by

$$\begin{aligned} P_{r1} &= \frac{S_{overlap} \times 50\% + (S_1 - S_{overlap}) \times 100\%}{S_1} \\ &= 1 - \frac{S_{overlap}}{2S_1}. \end{aligned} \tag{3.21}$$

Similarly, the recognition rate of object 2 is given by

$$P_{r1} = 1 - \frac{S_{overlap}}{2S_2} \tag{3.22}$$

Suppose that the speed ranges of objects 1 and 2 are $(v_{1,\min}, v_{1,\max})$ and $(v_{2,\min}, v_{2,\max})$, respectively. Assume that the two objects pass sufficiently many links over sufficient time. As shown in Fig. 3.29, the following four situations could occur.

- Case 1: $v_{2,\max} \geq v_{2,\min} \geq v_{1,\max} \geq v_{1,\min}$. In this case, there is no overlap. The recognition rate is 100%.

- Case 2: $v_{1,\max} \geq v_{2,\max} \geq v_{2,\min} \geq v_{1,\min}$. In this case, the area of object 2 is almost included in that of object 1. When N is large enough, the recognition rate is approximately 50% for object 2.

- Case 3: $v_{1,\max} \geq v_{1,\min} \geq v_{2,\max} \geq v_{2,\min}$. In this case, the overlap area is limited. When N is sufficiently large, the recognition rate is almost 100%.

- Case 4: $v_{2,\max} \geq v_{1,\max} \geq v_{2,\min} \geq v_{1,\min}$. When N is large, we can assume $t_{1,N} = t_{2,N} = t_N$ and thus obtain

$$\begin{aligned} S_{overlap} = & \quad (v_{1,\max} t_N - v_{2,\min} t_N - v_{1,\max} \Delta t) \\ \times & \quad (t_N - \tfrac{v_{1,\max} \Delta t}{v_{1,\max} - v_{2,\min}}) \\ = & \quad \tfrac{(v_{1,\max} t_N - v_{2,\min} t_N - v_{1,\max} \Delta t)^2}{(v_{1,\max} - v_{2,\min}) t_N}. \end{aligned} \tag{3.23}$$

The area of object 1 is given by $S_1 = (v_{1,\max} - v_{1,\min})(t_N - \Delta t)$. Hence, the recognition rate of object 1 is

$$P_{r1} = 1 - \frac{(v_{1,\max} t_N - v_{2,\min} t_N - v_{1,\max} \Delta t)^2}{(v_{1,\max} - v_{2,\min})(v_{1,\max} - v_{1,\min})(t_N - \Delta t) t_N}. \tag{3.24}$$

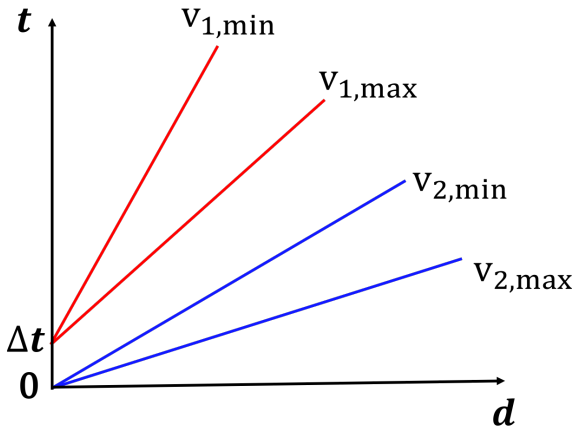


Figure 3.25: Case 1

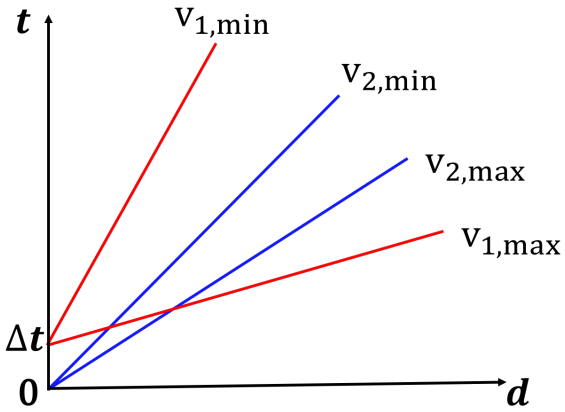


Figure 3.26: Case 2

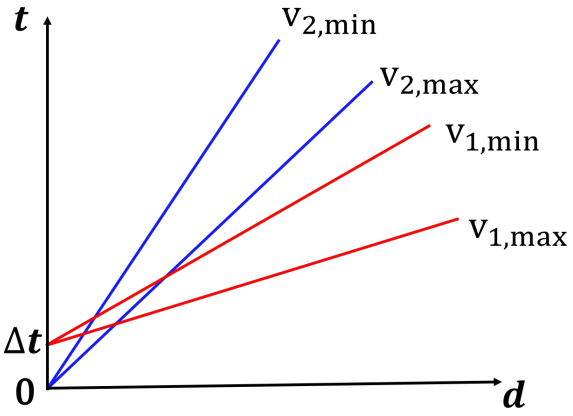


Figure 3.27: Case 3

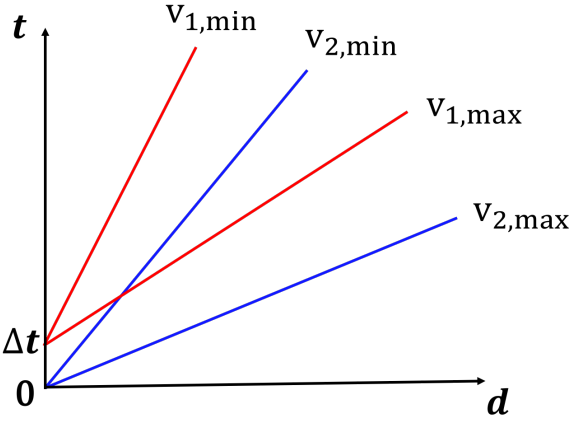


Figure 3.28: Case 4

Figure 3.29: Four cases of the scenario of two objects.

Similarly, the area of object 2 is $S_2 = (v_{2,\max} - v_{2,\min})t_N$. Therefore, the recognition rate of object 2 is

$$P_{r2} = 1 - \frac{(v_{1,\max}t_N - v_{2,\min}t_N - v_{1,\max}\Delta t)^2}{(v_{1,\max} - v_{2,\min})(v_{2,\max} - v_{2,\min})t_N^2}. \tag{3.25}$$

3.4.5 Numerical Simulations

We present numerical simulations on the proposed tracking algorithm using real trajectories. We use GPS to record walking trajectories of pedestrians. The accuracy of GPS data is about 1 meter, and the minimal time interval is 1 second, which are of sufficient precision for most applications. The millimeter wave communication links are randomly dropped in a certain region. The cases of two, three, and four objects are simulated. We first set all speed ranges to be same and change different starting times, which is shown in Fig. 3.30. The recognition rate increases with the starting time difference.

Then we fix the starting time difference and change the speed ranges. Fig. 3.31 shows the variation of the recognition rate with different speed ratios, namely the ratio between the speeds of different objects. At the beginning, the object starting earlier has a lower speed. When it has been caught up by other objects, they enter the overlapped region and thus cannot be recognized. As the speed ratio increases, the overlapped region becomes smaller and thus the recognition rate becomes higher. Moreover, in both figures, the more the objects are, the slower the recognition rate increases.

3.4.6 Conclusion

We have studied the tracking of moving object(s) by exploiting the blockage effect in millimeter communication networks. Both the short-term and long-term tracking problems have been studied, by leveraging the reflection-interference effect close to the LOS and the geometric image of distance-time plane, respectively. Based

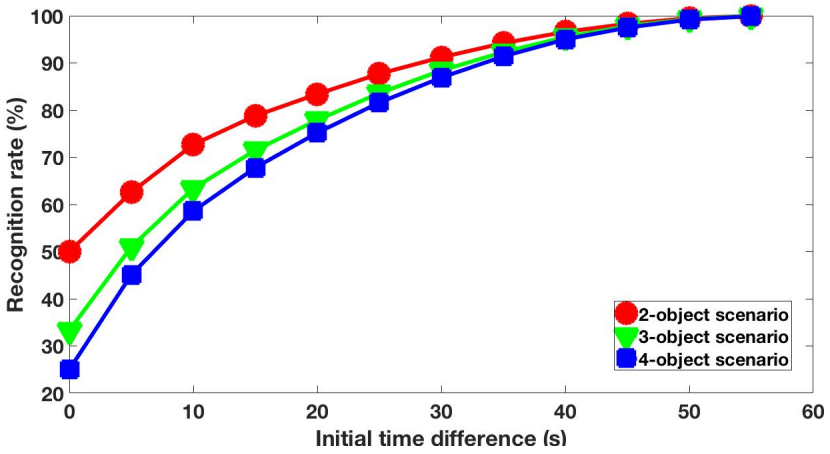


Figure 3.30: Recognition rate in term of starting time difference.

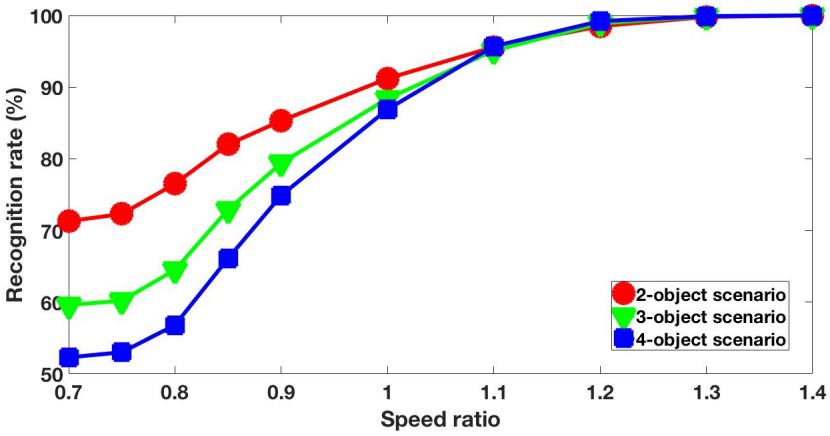


Figure 3.31: Recognition rate in term of speed ratio.

on experiments for a single link, numerical results have shown that the proposed algorithms are promising and may find potential applications in practice.

Chapter 4

Wind Sensing

In this chapter, we use Doppler effect in mmWave communication to estimate wind velocity [92].

4.1 Introduction

Compared with microwave in wireless communications, millimeter wave exhibits many advantages, particularly its large bandwidth. It is expected to be employed in 5G cellular communication networks [56] and vehicular networks [16]. Moreover, its short wavelength enables the integration of antenna array in both transmitter and receiver in the millimeter wave band. The antenna array can be used for various applications, particularly the beamforming which focuses power to a narrow angle, thus increasing the power efficiency and reducing the interference. Meanwhile, millimeter wave also provides a powerful machinery for sensing the environment, due to its directionality and fine spatial resolution. It has been widely used in automatic driving [26], radar imaging [10] and passive millimeter wave camera [84], and so on. A new application of millimeter wave is to carry out communications and sensing simultaneously. One approach is to reuse the same waveform for both communications and radar in the millimeter wave band [66]. The other approach is to add the functionality to millimeter wave communication systems as a 'bonus'. For

example, the blockage in millimeter wave communications can be used to detect and track mobile objects [94][91]. Another example is to leverage the spectrum sensing in the millimeter wave band for joint positioning [43]. Such a 'bonus' sensing scheme based on communications has also be used in the Wi-Fi band [29].

In this chapter, we propose to leverage the millimeter wave communications in the outdoor environment to sense wind velocity. This seems impossible at the first sight. However, it is based on the fact that millimeter wave communication devices are expected to be mounted to elevated locations such as lamp post, traffic light and high buildings. Such locations are subject to wind forces, which may cause significant oscillations of the fixtures. In the area of civil engineering there have been substantial studies on the wind impact on elastic poles and buildings [52][15]. The displacement of the fixtures could be in the scale of millimeters, or even more. This causes the change of radio propagation distance. In traditional microwave communications where the wavelength is in the order of centimeters or more, such a distance change of millimeter wave causes only negligible impact on the phase of communication signal. It is radically different in the millimeter wave band, where a displacement of 2.5mm may cause a phase change of π in the 60GHz band. Therefore, it is a new opportunity to use millimeter wave communications for the sensing of wind. On one hand, the information on wind is important for environment monitoring; on the other hand, the measurement on the oscillation of poles and buildings is also important for the corresponding structure monitoring in civil engineering. There have been dedicated devices for wind speed measurement. In [41], a laser Doppler radar is used to measure the atmospheric wind velocity remotely. [85] built a theoretical model by using GPS signals from the ocean to determine wind speed. Later, [38] developed an all-fiber pulsed coherent Doppler Lidar system for wind sensing.

The order of price of commercial anemometer is hundreds of dollars, along with communication equipments, installation and maintenance. To achieve the same deployment density as 5G devices, the cost will be very high. For comparison, the data for wind estimation in our proposed algorithm is the communication signal

itself. Therefore, the millimeter wave communication infrastructure is 'free' for the wind monitoring, it waives of the substantial cost of mounting new wind sensors as well as the sensor network.

4.2 Doppler Shift and Amplitude Modulation

In this section, we analyze the doppler shift and amplitude modulation incurred by the wind-triggered oscillation of millimeter wave fixtures. For simplicity, we focus on the receiver. The analysis is the same for the transmitter.

4.2.1 Force and Motion Model

We assume that the millimeter wave receiver, fixed in a box, is mounted to a pole as illustrated in Fig. 4.1. It is subject to wind, which causes the oscillation of the pole and thus that of the millimeter receiver. It is well known that the wind energy is the kinetic energy generated by air motion. According to [52], the wind power through a surface during time period t is given by $P = \frac{1}{2}S\rho v^3$, where v is the wind speed component in the direction of line of sight (LOS), ρ is the density of air, and S is perpendicular force-bearing area of the box along the direction of the wind, and the force of wind is given by $F = \frac{1}{2}S\rho v^2$.

For simplicity of analysis, we assume the end-loaded cantilever pole for the millimeter wave receiver and the pole, namely all the mass is focused in the receiver box. According to [15], the elastic deflection at the end is given by

$$\delta = \frac{FL^3}{3EI}, \tag{4.1}$$

where L is the length of pole, E is modulus of elasticity, and I is the area moment of inertia of the pole's cross section.

Note that, in the experiment elated in Section 4.4, we find that actual motion of the box is extremely complicated subject to wind. For the essence of the analysis, a simple

harmonic motion is a reasonable assumption to describe the motion approximately. The speed of harmonic motion is given by

$$v_{sh}(t) = A_{sh} \sin(w_0 t + \phi_{sh}), \tag{4.2}$$

where ϕ_{sh} is the initial phase, A_{sh} is the amplitude, which is equal to the elastic deflection given by $A_{sh} = \delta$, and w_0 is the angular frequency of harmonic motion, which is given by $w_0 = \sqrt{\frac{k}{m}}$, where k is the spring constant for a mass on a elastic beam, m is the inertial mass of the box.

4.2.2 Doppler Shift

The Doppler effect is a phenomenon in which the observer receives the wave at a frequency different from the frequency of the wave source, when the wave source and the observer have a relative motion. In our context, the relationship between received frequency f_r and transmitted frequency f_t is given by

$$f_r = \frac{c \pm v_{sh}}{c \pm v_t} f_t, \tag{4.3}$$

where c is the light speed velocity, v_{sh} is the velocity of the receiver antenna in harmonic motion in (4.2), whose sign indicates the direction of movement (to or from the receiver) and v_t is the velocity of the transmitter, which is 0 in our context.

As a result, the frequency difference between the transmitter and receiver is given by

$$\begin{aligned} \Delta f &= f_r - f_t = \frac{v_{sh}}{c} f_t \\ &= \frac{S\rho v^2 L^3 w \sin(w_0 t + \phi_{sh})}{6EIc} f_t \\ &= A \sin(w_0 t + \phi_{sh}), \end{aligned} \tag{4.4}$$

where the amplitude A is given by

$$A = \frac{S\rho v^2 L^3 w_0 f_t}{6EIc}. \tag{4.5}$$

Therefore the frequency oscillation due to the Doppler shift and wind-driven oscillation is also a harmonic motion. The corresponding variance is then given by

$$\begin{aligned} var_{\Delta f} &= \int_{\phi_{sh}}^{2\pi+\phi_{sh}} A^2 \sin(x+\phi_{sh})^2 \frac{1}{2\pi} dx \\ &= \frac{A^2}{2\pi}\left(\frac{1}{2}x - \frac{1}{4}\sin(2x+\phi_{sh})\right)\Bigg|_{\phi_{sh}}^{2\pi+\phi_{sh}} \\ &= \frac{S^2\rho^2 v^4 L^6 w_0^2 f_t^2}{72E^2 I^2 c^2} \propto v^4 \end{aligned} \tag{4.6}$$

Therefore, the wind speed component on then direction of LOS is

$$v = \left(2var_{\Delta f}\right)^{\frac{1}{4}} \left(\frac{6EIc}{S\rho L^3 w_0 f_t}\right)^{\frac{1}{2}}. \tag{4.7}$$

If the model is precise and all the parameters of the pole are known, we estimate the wind speed by measuring the variance of the Doppler shift. It may be difficult to obtain the parameters of the pole; however, at least we can show $var_{\Delta f} \propto v^4$, both theoretically and experimentally. If a reference wind speed, as well as the variance of Doppler shift is known, we can estimate v from the measurement of $var_{\Delta f}$.

4.2.3 Amplitude Modulation

The second way to understand the impact of oscillation on the millimeter wave communications is to consider the amplitude modulation due to the change of propagation distance. At the transmitter end, we assume a single-tone baseband signal, which is given by $s_m(t) = \cos w_m t$, where the amplitude is normalized for simplicity. The carrier signal is given by $s_c(t) = \cos w_c t$, where w_c is the carrier

frequency in the millimeter wave band. Hence, the modulated signal is given by

$$s_m(t)s_c(t) = \cos w_m t \; cosw_c t \tag{4.8}$$

which is emitted through antenna.

During the propagation, the phase increment is given by

$$\phi(t) = \frac{x(t)}{\lambda} = \frac{A\cos(w_0 t)}{\lambda} + \phi_0, \tag{4.9}$$

where $x(t)$ is the time varying propagation distance, which is given by

$$x(t) = A\cos(w_0 t) + x_0, \tag{4.10}$$

where x_0 is the distance when there is no wind, and ϕ_0 is given by $\frac{x_0}{\lambda}$.

At the receiver end, when the receiver uses local carrier $\cos w_c t$ (suppose that there is no phase lock loop (PLL), or the PLL cannot catch up with the phase oscillation due to the wind). Then, the demodulation output is given by

$$m_d(t) \propto \cos w_m t \cos\phi(t), \tag{4.11}$$

where the term $\cos\phi(t)$ changes much slower than the message signal frequency w_m. Therefore, we can consider $\cos\phi(t)$ as an amplitude modulation to the message signal $\cos w_m t$.

Note that the frequency change due to Doppler shift is very small due to the slow speed of oscillation when compared with the light speed. Therefore, the impact of wind-driven oscillation on the millimeter wave communications can be considered as a narrow band frequency modulation. It is well known that a narrow band frequency modulation is approximately the same as amplitude modulation [40]. Therefore, the above two explanations, namely the frequency Doppler shift and amplitude modulation due to the propagation distance change, are essentially the same.

4.3 Wind Velocity Estimation

In this section, we propose an algorithm to estimate the wind velocity based on the analysis between the wind speed and frequency oscillation in the millimeter wave communications discussed in the previous section. The major challenge is how to estimate the direction of the wind, since the speed can be estimated using the variance of the frequency oscillation. It is impossible to estimate the wind direction based on only the frequency variance values, since only the velocity component along the LOS accounts for the frequency variance, as will be demonstrated in the experiments. Therefore, we leverage the antenna arrays and multiple simultaneous beams in millimeter wave communications.

4.3.1 Mathematical Model

We assume that the speed and direction of wind are constants within a small period, which are denoted by v and θ. There are N millimeter wave beams at the millimeter wave transmitter (or receiver), whose directions are $\theta_1, ..., \theta_N$. During this coherence time of wind, the wind velocity components along the N millimeter wave beams direction are denoted by $\{v_1, ..., v_N\}$, respectively.

As illustrated in Fig. 4.2, one beam i has direction θ_i and the corresponding wind velocity component is v_i, while another beam j has angle θ_j and wind velocity component v_j. The angle of wind direction is denoted by θ. Then we have

$$\begin{cases} v_i = (-1)^{m_i} v \cos(\theta - \theta_i) \\ v_j = (-1)^{m_j} v \cos(\theta - \theta_j) \end{cases}, \tag{4.12}$$

where for $k = i, j$,

$$m_k = \begin{cases} 0, & \min(|\theta - \theta_k|, 360^\circ - |\theta - \theta_k|) <= 90^\circ \\ 1, & \text{otherwise.} \end{cases}$$

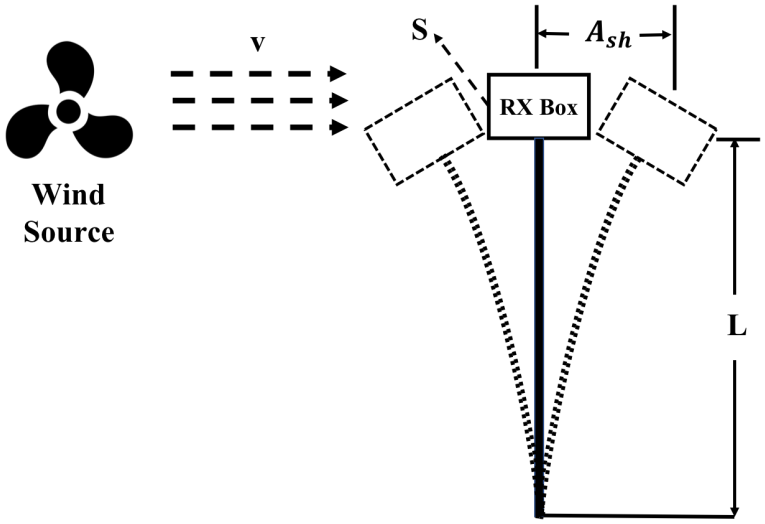


Figure 4.1: Force and motion illustration.

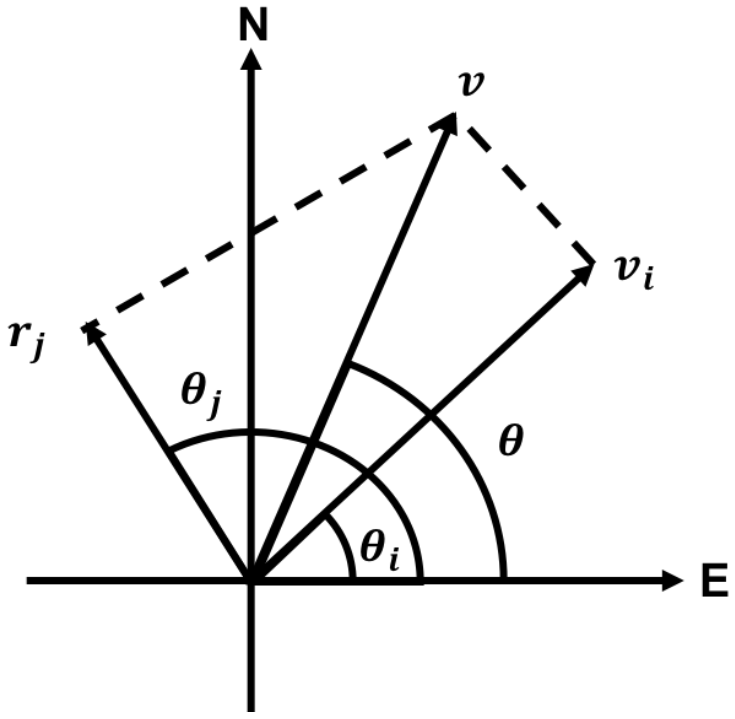


Figure 4.2: Two antennas and wind velocity.

As a result, we can obtain the estimations of the wind direction θ_{ij} and the wind speed v_{ij} from the the local estimation of wind speeds v_i and v_j at beams i and j, as well as their own direction θ_i and θ_j:

$$\theta_{ij} = \tan^{-1} \frac{v_i \cos\theta_j - v_j \cos\theta_i}{v_j \sin\theta_i - v_i \sin\theta_j} \tag{4.13}$$

and

$$v_{ij} = \frac{\sqrt{v_i^2 - 2v_i v_j \cos(\theta_i - \theta_j) + v_j^2}}{|\sin(\theta_i - \theta_j)|}. \tag{4.14}$$

We observe that the wind direction and speed (thus the velocity) can be estimated from the measurements at two beams. When we have more than two beams, we can simply compute the average of the estimations for all possible beam pairs.

4.3.2 Algorithm

The detailed algorithm for the wind velocity estimation is summarized in Algorithm 4.

1: Calculate wind speed component $\{v_1, ..., v_N\}$ on N beam directions $\{\theta_1, ..., \theta_N\}$.
2: **for** $i = 1, ..., N-1$ **do**
3: **for** $j = i+1, ..., N$ **do**
4: **if** $mod(\theta_i - \theta_j, 180°)! = 0$ **then**
5: Calculate θ_{ij} and v_{ij} using (4.13) and (4.14).
6: **end if**
7: **end for**
8: **end for**
9: Estimated the direction using $\hat{\theta} = \frac{\sum_{j=i+1}^{N} \sum_{i=1}^{N-1} \theta_{ij}}{C_N^2}$.
10: Estimated the speed using $\hat{v} = \frac{\sum_{j=i+1}^{N} \sum_{i=1}^{N-1} v_{ij}}{C_N^2}$.

Algorithm 4: Wind velocity estimation subject to N beams

4.4 Experiment and Simulations

In this section, we study the Doppler effect caused by wind in millimeter wave communications, by using hardware testbed in the 60GHz band. We will first introduce the devices used in the testbed, and then explain the experiment procedure. Then the experiment results will be given in details. Finally, we provide numerical simulation results on the wind velocity estimation.

4.4.1 Testbed

We build the communication link by using the Analog Devices EK1HMC6350 evaluation kit, which provides half-duplex, 60 GHz millimeter wave. One board is used as transmitter (TX) and the other one as receiver (RX). Both have horn antennas with a 3dB angle of 10°. We use Tektronix AFG3102C, a dual channel arbitrary/function waveform generator, as the baseband signal source. We use laptops to program and control the entire communication link by a graphical user interface (GUI) software and a USB interface.

We use E1200 standard tuned propulsion system made by SZ DJI Technology Co., Ltd. as the wind source, as shown in Fig. 4.4. The system includes 4216 motors, 40A smart ESCs (Electronic Speed Control), and 17-inch ultra-carbon folding propellers. It can provide up to 1040W of power, and generate wind with speed 10m/s at the distance of 1.5 meters.

4.4.2 Experiment Procedure

A live picture of the experiment is shown in Fig. 4.5. The experiment procedure is illustrated in Fig. 4.6.

1. We fix the RX board and antenna in a windproof box and mount the box to one end of an elastic pole. The other end of the pole is fixed to the ground.

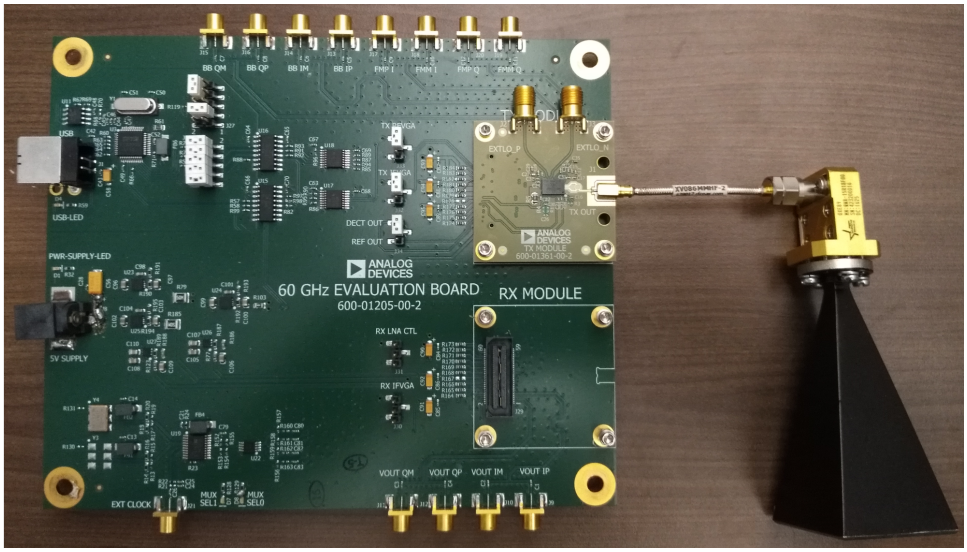


Figure 4.3: Analog Devices EK1HMC6350 board with antenna.



Figure 4.4: DJI E1200 standard tuned propulsion system.

2. We start the propulsion system to generate wind at a constant speed. The direction of wind has a preset angle to the LOS between TX and RX.

3. The source generates a 1MHz sinusoidal baseband signal. The TX board up-converts the baseband signal to the 60GHz band, and emits through the antenna.

4. The RX board down-converts the received signal.

5. Laptops control the boards and store sufficiently many samples of the demodulated signal for further analysis.

During the experiment, we notice that the wind passing through the up-conversion board causes a significant frequency shift, as shown by the dotted curve in Fig. 4.8. After a thorough examination, we found that the reason is the temperature drop due to the wind and the subsequent frequency drift of the crystal oscillation (which is sensitive to the temperature). Although the frequency drift is marginal (in the order of kHz) when compared with the carrier frequency, it dominates the frequency change due to the wind-driven oscillation, thus making the wind velocity estimation very noisy. To eliminate the effect of frequency shift due to the temperature change, we put the receiver board and antenna into a sealed box to create a windless environment.

4.4.3 Data Processing

The received signals are sampled with the sampling rate of 20M samples/second after down-conversion. Then, the samples are divided into blocks of 200k samples. Fast Fourier Transform (FFT) is used to estimate the signal spectrum. The frequency of peak spectrum amplitude is selected as the instantaneous frequency.

To further remove the long-term drift of frequency, we use nonlinear regression to remove the drift. We divide the data into segments of ten seconds. In each segment, we use the quadratic regression $f(t) = p_1 t^2 + p_2 t + p_3$, as shown in Fig. 4.7, where p_1, p_2 and p_3 are coefficients to be estimated. Once the nonlinear regression is completed,

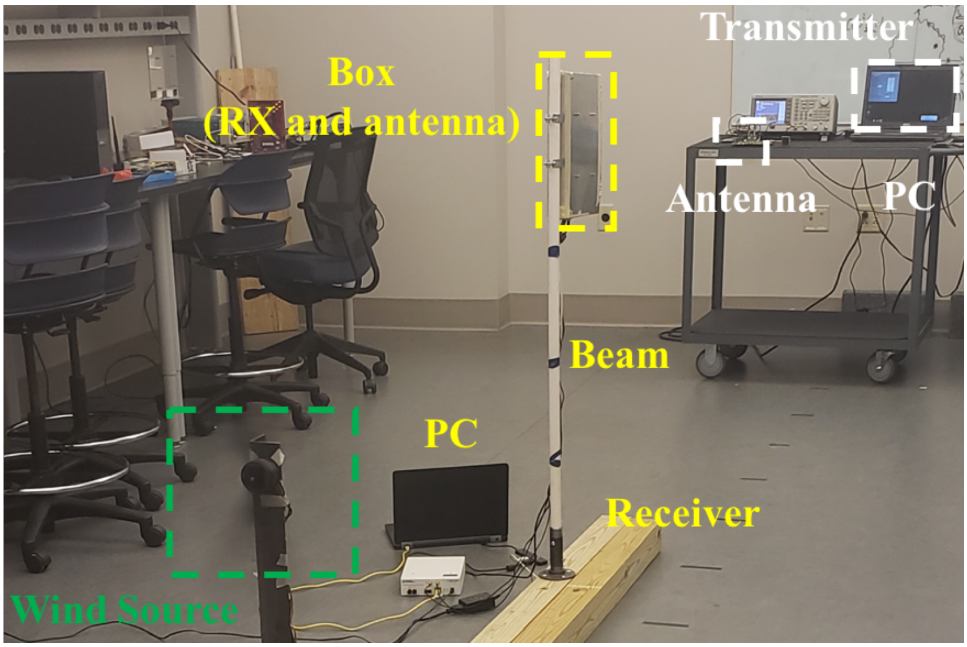


Figure 4.5: Live picture of the experiment.

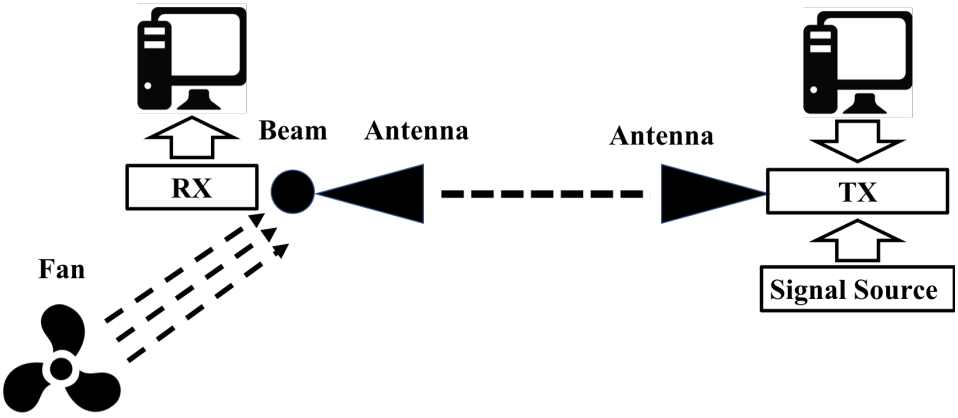


Figure 4.6: The experiment setup

we remove the prediction from the nonlinear regression, such that only the frequency oscillation remains. The frequency oscillation after the drift removal is then shown by the solid curve in Fig. 4.8. A finer waveform is shown in Fig. 4.9. We can observe that in the local time scale there exists an oscillation of the frequency, as predicted in our mathematical model.

4.4.4 Experimental Results

In the experiments, we repeat the above procedure for three wind speeds (2.6m/s, 5.0m/s, 7.7m/s) on four directions (0°, 30°, 60°, 90°) to the LOS. By evaluating the variance of the samples we have obtained in the experiments, we show the frequency variances versus the fourth power of wind speed (v^4) in Fig. 4.10.

From the figure, we can draw the following conclusions:

- The variance of frequency increases with the wind speed, and is approximately proportional to the fourth power of wind speed, which coincide with our theoretical prediction.
- Only the component of the wind velocity in the direction of LOS causes Doppler shift and thus the frequency oscillation. The variance of frequency decreases as the angel between the wind and LOS ranges from 0° to 90°.
- The frequency oscillation is much more chaotic than the simple model based prediction. However, the model has well predicted the law of fourth power of wind speed, as discussed above, which shows the validity of the model.

4.4.5 Numerical Simulation

Based on the experimental results, we carry out simulations for Algorithm 4. For any communication beam, wind speed component estimation using (4.7) is subject to errors due to noise and imperfections in the modeling. The smaller the angle between the LOS and wind direction has, the larger the error will be, due to the decreasing

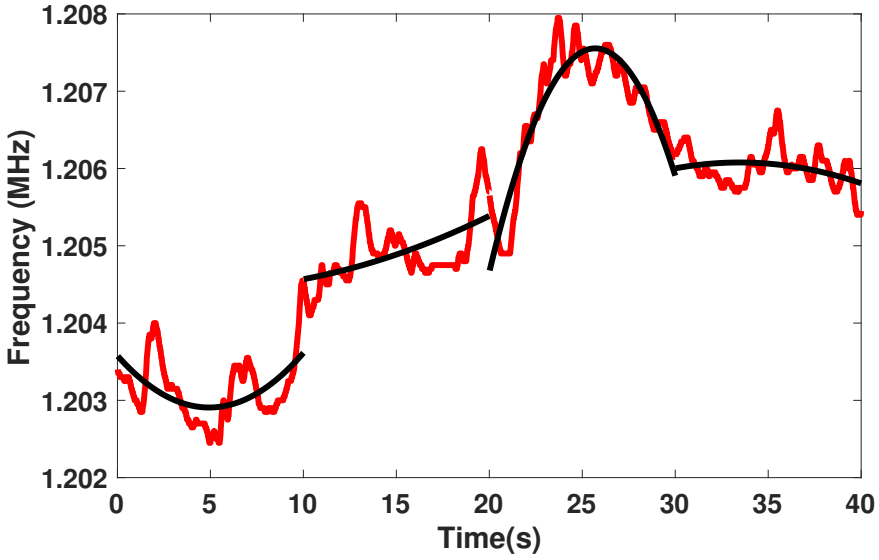


Figure 4.7: Curve fitting for evaluating the frequency oscillation.

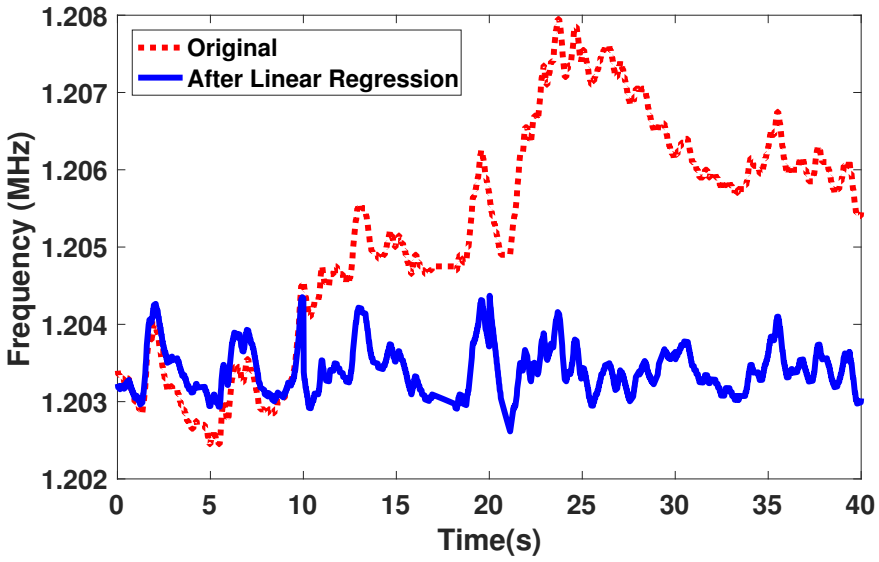


Figure 4.8: Frequency shifts in the demodulated signal over time.

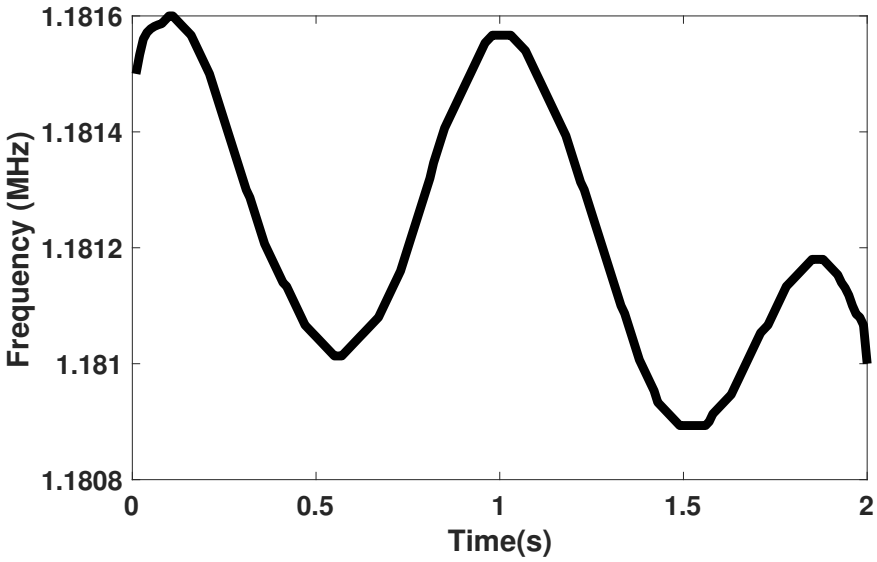


Figure 4.9: Frequency shift in finer time scale.

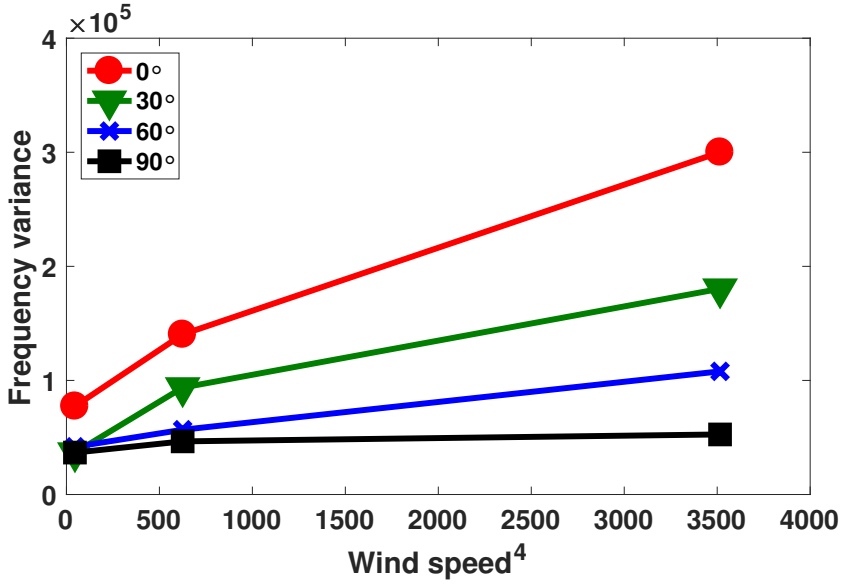


Figure 4.10: Frequency variance in different wind speeds and directions.

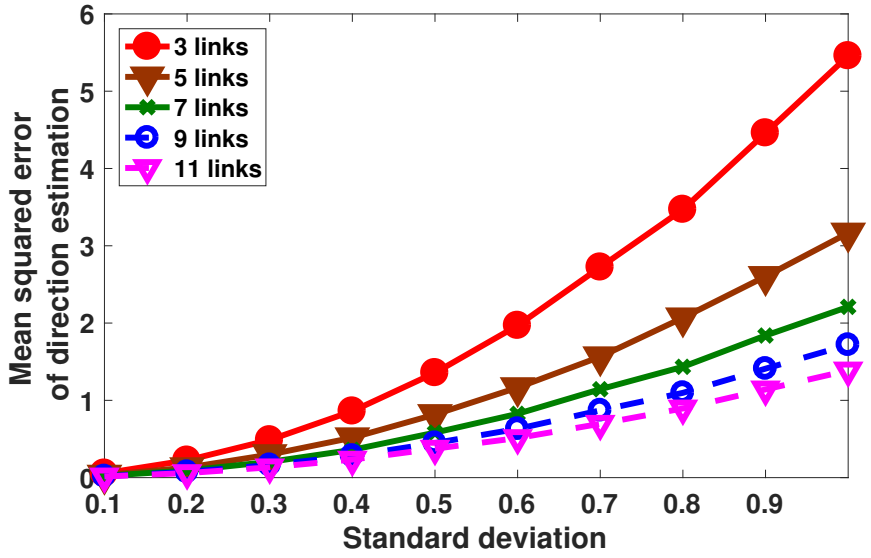


Figure 4.11: Mean squared error of wind direction estimation.

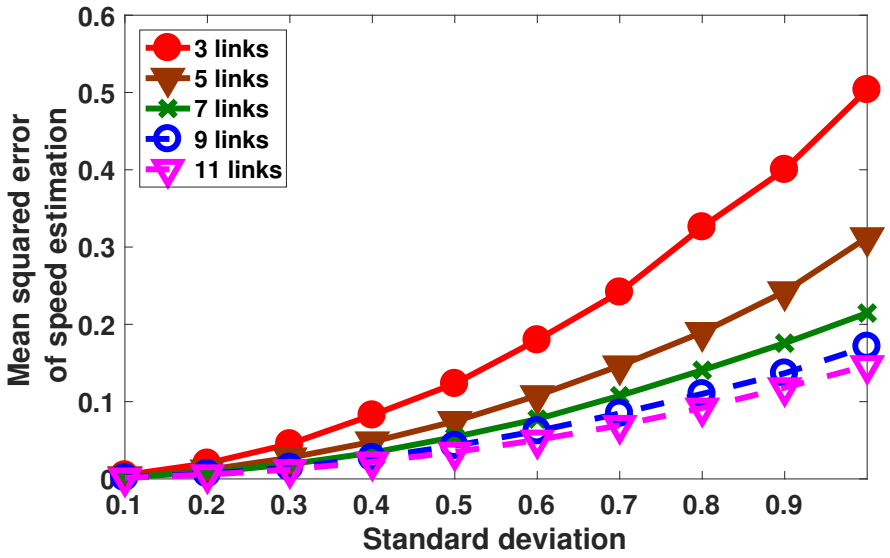


Figure 4.12: Mean squared error of wind speed estimation.

signal-to-noise-ratio (SNR). We assume that the speed component estimation in direction $i, i \in 1, ..., N$ obeys normal distribution $\mathcal{N}(v_i, \cos(\theta - \theta_i)\sigma)$, where σ is a positive number common to all beams.

We calculate the mean squared error (MSE) of the wind direction and speed estimations with increasing number of beams ranging from 3 to 11, as well as the noise power σ from 0.1 to 1. The simulation results are shown in Figures 4.11 and 4.12. We conclude that increasing the number of beams can substantially reduce the MSE of both estimations.

4.5 Conclusion

We have carried out experiments to examine the Doppler effect caused by wind in the millimeter wave band. The results have shown that a frequency oscillation can be easily detected in the demodulated signal. We have proposed an algorithm to calculate wind speed component, and thus the wind velocity (speed and direction). We have carried out an experiment in the 60GHz band to demonstrate the theoretical prediction, and the outcome matches the theoretical model quite well. Numerical simulations have been carried out to evaluate the performance of wind velocity estimation.

Chapter 5

Optical-like Properity Study of mmWave

Since the wavelength of mmWave is close to visible light, it has optical-like propagation characteristics. Meanwhile, we accidentally find an oscillation phenomenon during blockage experiments [90]. Both are useful to remotely sense.

5.1 Oscillation

In the experiments in chapter 3, we observe oscillations before and after the full blockage, which is shown in Fig. 5.1. To the best of our knowledge, such a phenomenon has not been reported in existing literature before. Before we leverage this phenomenon for speed and position estimations of the object, we first explain the underlying mechanism of generating such oscillations.

The mechanism of the oscillations before and after the blockage is illustrated in Fig. 5.2. When an object is close to the LOS, it causes a Non-LOS (NLOS) reflection, thus incurring interference with the LOS signal at the receiver. With the phase change of the NLOS signal, due to the changing propagation distance caused by the moving

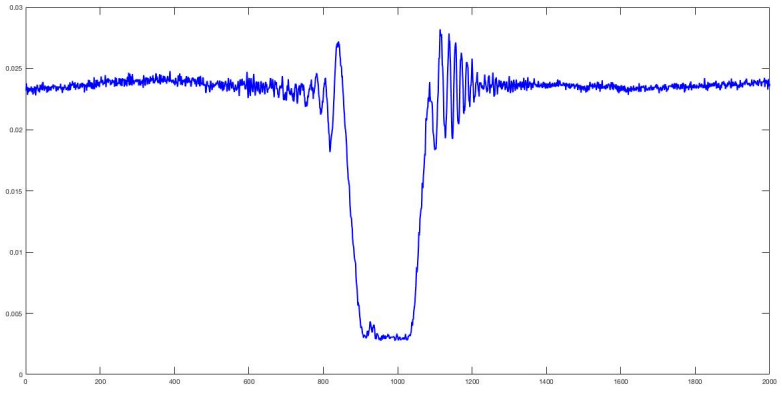


Figure 5.1: Variation and oscillations of signal strength before and after a blockage.

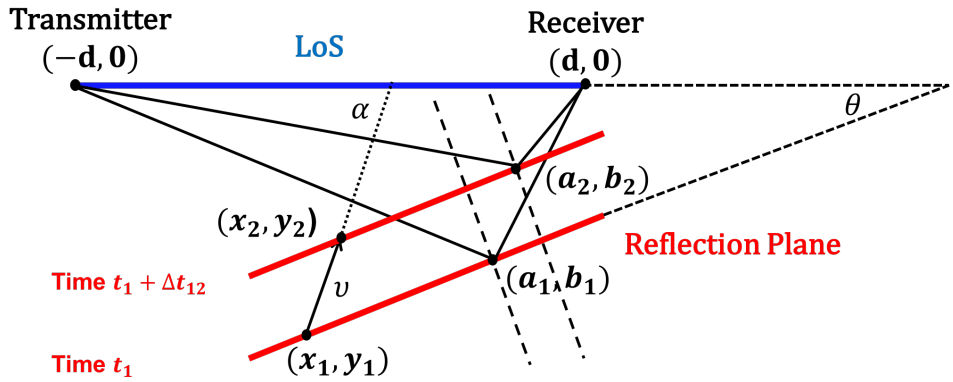


Figure 5.2: Mechanism of oscillations before and after the blockage.

object, the signal at the receiver is either enhanced or weakened. One period of the oscillation is achieved when the reflection path distance is changed by one wavelength.

In more mathematical details, the signal strength at time t is given by

$$s(t) = Re\left[A_{LOS}e^{j\theta_{LOS}} + A_f e^{j\theta_f(t)}\right], \tag{5.1}$$

where A_{LOS} and θ_{LOS} are the amplitude and phase of the LOS signal, respectively, and A_f and $\theta_f(t)$ are those of the reflection path. Since the movement is tiny, it is reasonable to assume that only the phase of the reflection path changes with time, thus being a function of t. Then, at time $t+\tau$, when the propagation path distance is changed by δd due to the movement of the object, the signal strength is changed to

$$s(t+\tau) = Re\left[A_{LOS}e^{j\theta_{LOS}} + A_f e^{j\theta_f(t)+2\pi\frac{\delta d}{\lambda}}\right], \tag{5.2}$$

where λ is the wavelength of the millimeter wave. Obviously, when $\delta d = \lambda$, we have $s(t) = s(t+\tau)$, thus achieving one period of oscillation.

5.1.1 Tracking Algorithm

An interesting application of the oscillation phenomenon is the tracking of the intruding object (only when it is close to the LOS), by estimating its location and speed using the samples in the oscillation period. Below is the mathematical analysis and algorithm.

Due to the small wavelength of millimeter wave, the reflection surface can be approximated by a plane. As shown in Fig. 5.2, at time t_1, we denote the coordinates of transmitter, receiver, reflection point and a known point on the reflection plane by $(-d, 0)$, $(d, 0)$, (a_1, b_1) and (x_1, y_1), respectively. Denote the blockage range by $[-y_b, y_b]$, then $|y| > |y_b|$. The angle between the LoS and reflection plane is denoted by $\theta, \theta \in [0, \frac{\theta_a}{2}]$. By using trigonometric functions, the coordinate of the mirror

point of $(d, 0)$ (i.e., the receiver position) with respect to the reflection plane is $(\frac{d-2y_1\tan\theta+(2x_1-d)\tan^2\theta}{1+\tan^2\theta}, \frac{2y_1+2(d-x_1)\tan\theta}{1+\tan^2\theta})$. Then the coordinate of the reflection point, (a_1, b_1), is given by

$$\begin{cases} a_1 = & \frac{(d^2+y_1^2)\tan\theta-2x_1y_1\tan^2\theta+x_1^2\tan^3\theta}{x_1\tan\theta-y_1\tan^2\theta+x_1\tan^3\theta-y_1} \\ b_1 = & \frac{(d^2-x_1^2)\tan^2\theta+2x_1y_1\tan\theta-y_1^2}{x_1\tan\theta-y_1\tan^2\theta+x\tan^3\theta-y_1}. \end{cases} . \tag{5.3}$$

Hence, the length of reflection path r_1, from the transmitter to the receiver, at time t_1 is given by

$$r_1 = \sqrt{(a_1+d)^2+b_1^2} + \sqrt{(a_1-d)^2+b_1^2}. \tag{5.4}$$

Now, we assume that the object moves to (x_2, y_2) over time Δt_{12} with a speed v. The corresponding reflection point is changed to (a_2, b_2). The angle between direction of object movement and LoS is α. Since Δt is very small, it is assumed that θ remains the same. Based on these assumptions, (x_2, y_2) can be calculated from the following equations:

$$\begin{cases} x_2 = x_1 + vt_{12}cos\alpha \\ y_2 = y_1 + vt_{12}sin\alpha \end{cases} . \tag{5.5}$$

Replacing (x_1, y_1) with (x_2, y_2) in Equations (5.3), we can obtain (a_2, b_2). Hence, the length of reflection path r_2 at time $t_2 = t_1 + \Delta t_{12}$ is given by

$$r_2 = \sqrt{(a_2+d)^2+b_2^2} + \sqrt{(a_2-d)^2+b_2^2}, \tag{5.6}$$

from which the length difference of the reflection paths, Δr_{12}, over time Δt_{12} is given by

$$\begin{aligned} \Delta r_{1,2} = \quad & |\sqrt{(a_1+d)^2+b_1^2} + \sqrt{(a_1-d)^2+b_1^2} \\ & -\sqrt{(a_2+d)^2+b_2^2} - \sqrt{(a_2-d)^2+b_2^2}|, \end{aligned} \tag{5.7}$$

which is a function of variables $x_1, y_1, v, \alpha, \theta$.

According to the mechanism of oscillation explained in the last subsection, when $\Delta r_{1,2}$ is equal to one waveform, the signal strength is repeated. Hence, we can choose six time snapshots, t_i, $i = 1, 2, 3, 4, 5, 6$, such that the corresponding received signal strengths are identical. The corresponding path differences are denoted by $\Delta r_{i,i+1}(x_1, y_1, v, \alpha, \theta)$. Therefore, we obtain the following five nonlinear equations:

$$\Delta r_{i,i+1}(x_1, y_1, v, \alpha, \theta) = \lambda, \qquad i = 1, ..., 5. \tag{5.8}$$

By solving the five equations, we can obtain the five unknowns $x_1, y_1, v, \alpha, \theta$, thus recovering the trajectory. Note that due to the symmetry of the LOS and the middle point of LOS, there are four symmetric solutions to (5.8), as illustrated in Fig. 5.3.

The entire algorithm is summarized in Algorithm 5.

1: Obtain the durations of five consequent periods of oscillation, denoted by Δt_{12}, Δt_{23}, Δt_{34}, Δt_{45}, Δt_{56}.

2: Establish the five equations in (5.8).

3: Solve the equations to obtain $x_1, y_1, v, \alpha, \theta$.

4: Using the initial position, speed and angle to reconstruct the trajectory.

Algorithm 5: Tracking Algorithm based on Oscillation

5.1.2 Verification

We verify the proposed algorithm in Algorithm 5 by simulations using real measurements. Note that it is difficult to obtain measurements for high speed objects. Hence, we use the real experiment measurements for the time intervals in the case of 1m/s. For the other cases of speed, the time intervals are obtained by compressing those of 1m/s case accordingly. The parameters of the experiment are shown in Table 5.1.

The comparison of the true values and the estimations is shown in Table 5.2. It is observed that the estimation error is reasonably small. The error is due to measurement noise and the imprecise assumptions (e.g., the reflection plane angle

does not change and the object moves in straight line). Hence, the proposed scheme can be used to extract useful information of the moving object in practice.

5.2 Reflection

In chapter 3, we detect a ground reflection with 25dB attenuation in experiments. Though it can be ignored in blockage phenomenon, it is still important in mmWave communication. We study the characteristics of different materials by carrying out a series of experiments.

5.2.1 Experiment procedure

Testbed is described in Section 3.2.1. As shown in Fig. 5.4, the procedure is [42]:

1. The signal source generates a 100MHz sinusoidal baseband signal and transfer it to the transmitter.
2. The transmitter up-converts the input signal to 60GHz and emits via the antenna.
3. The 60GHz signal is scattered on the surface of an object somewhere in propagation.
4. The receiver down-converts the received signal and displays the demodulated baseband signal on the oscilloscope.
5. The receiver keeps moving circularly in the center of the object and stops at a location where the amplitude of the received signal is maximum. Record the angle between transmitter and receiver with respect to the object.
6. Rotate the object by a tiny degree, and repeat 1 - 5.

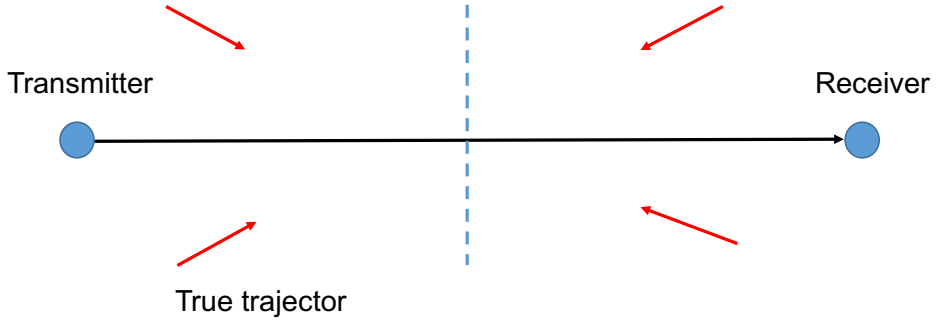


Figure 5.3: Four possible solutions to Eq. (5.8).

Table 5.1: Parameters measurements.

Transceiver distance $2d$	3m
Blockage range $[-y_b, y_b]$	[-0.2m, 0.2m]
Antenna's flare angle θ_a	15°
Millimeter wavelength λ	0.005 m
Initial location x_1	0 m
Initial location y_1	-0.2 m
Angle α	90°
Angle θ	0°

Table 5.2: Comparison of actual and estimated values.

Actual speed (m/s)	1	3	5	10	15	20
Est. speed (m/s)	0.69	2.19	3.93	7.71	10.95	15.42
Est. x_1(m)	-0.67	-1.11	-1.56	-0.67	-1.11	-0.67
Est. y_1(m)	-0.24	-0.23	-0.22	-0.21	-0.23	0.21
Est. $\alpha(^\circ)$	90	90	70	63	90	63
Est. $\theta(^\circ)$	5	4.2	3.3	3.3	4.2	3.3

We repeat the experiment in scenarios of different reflection surfaces, including human being, iron cabinet, vehicle side and corner. After calculation, signal-to-noise ratio (SNR) for different angle is plotted in Fig. 5.5, in which we can conclude that:

- The reflected signal of metal surface is significantly strong.
- Energy loss on metal surface is much less than that on human being.
- The smoother the object surface is, the smaller angle range the scattered signal is concentrated in.

5.2.2 Problem Formulation

For a single reflection event, assume the coordinate, angle of antenna, time of transmitter and receiver are $\{(x_1, y_1), \theta_1, t_1\}, \{(x_2, y_2), \theta_2, t_2\}$, respectively. The slope are $a_1 = \tan\theta_1, a_2 = \tan\theta_2$. Then the coordinate of the intersection point is

$$\left(\frac{a_1x_1 - a_2x_2 - y_1 + y_2}{a_1 - a_2}, \frac{a_1y_2 - a_2y_1 + a_1a_2x_1 - a_1a_2x_2}{a_1 - a_2}\right). \tag{5.9}$$

Meanwhile, the time of intersection is

$$t = \frac{At_2 - Bt_2}{A + B}, \tag{5.10}$$

where

$$A = \left((a_2x_1 - a_2x_2 - y_1 + y_2)^2 + (a_1y_2 - a_1y_1 + a_1a_2x_1 - a_1a_2x_2)^2\right)^{\frac{1}{2}} \tag{5.11}$$

$$B = \left((a_1x_1 - a_1x_2 - y_1 + y_2)^2 + (a_2y_2 - a_2y_1 + a_1a_2x_1 - a_1a_2x_2)^2\right)^{\frac{1}{2}} \tag{5.12}$$

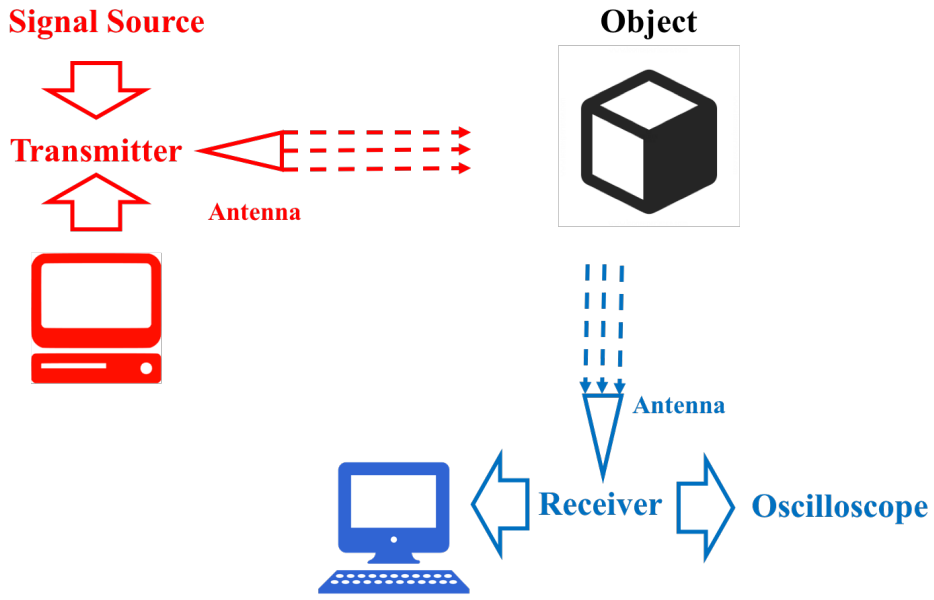


Figure 5.4: Experiment procedure.

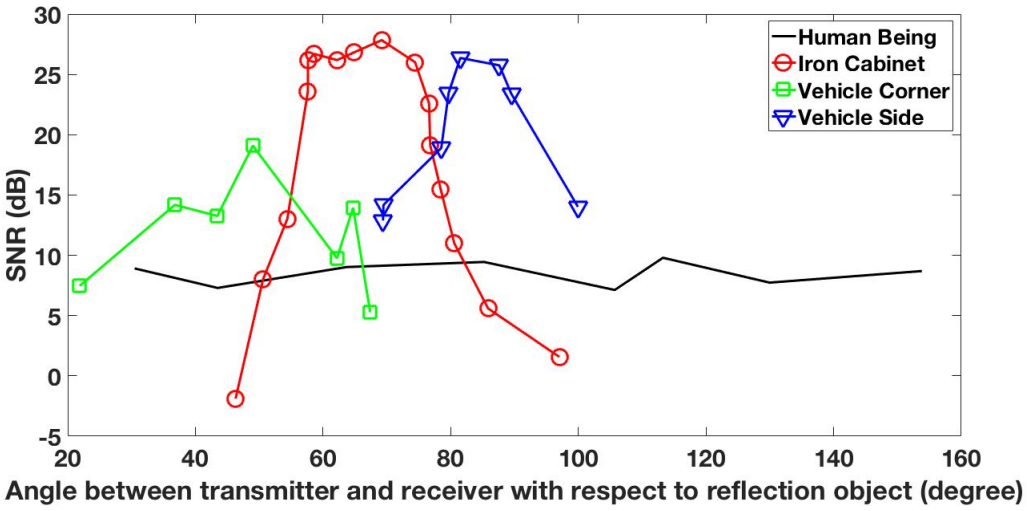


Figure 5.5: SNR in terms of angle.

5.2.3 Tracking Algorithm based on Kalman Filter

In this section, we track the trajectory of the blockage object based on the Kalman filter. In practical millimeter communication system, a base station receives both direct and reflected transmission signals. Since the angular range of the transmission is very small, it is easy to narrow down the possible range where the reflection happens, and figure out the most possible reflection coordinate and time. Our goal is to estimate the trajectory of the object. Assume that we have n calculated reflection event coordinates $\{(x_1, y_1), (x_2, y_2), ..., (x_n, y_n)\}$ and corresponding times $\{t_1, t_2, ..., t_n\}$. The state of the object at a time includes coordinate, speed, and acceleration. The initial state is

$$X_0 = [x_2; y_2; \frac{x_2 - x_1}{t_2 - t_1}; \frac{y_2 - y_1}{t_2 - t_1}; \frac{x_2 - x_1}{(t_2 - t_1)^2}; \frac{y_2 - y_1}{(t_2 - t_1)^2}]. \tag{5.13}$$

Meanwhile, the initial error covariance matrix, state-transition matrix, observation matrix, the covariance of the observation noise and the covariance of the process noise are, respectively:

$$P_0 = \begin{bmatrix} 1 & 0 & 0 & 0 & 0 & 0 \\ 0 & 1 & 0 & 0 & 0 & 0 \\ 0 & 0 & 10 & 0 & 0 & 0 \\ 0 & 0 & 0 & 10 & 0 & 0 \\ 0 & 0 & 0 & 0 & 10 & 0 \\ 0 & 0 & 0 & 0 & 0 & 10 \end{bmatrix}$$

$$F = \begin{bmatrix} 1 & 0 & t_2 - t_1 & 0 & (t_2 - t_1)^2/2 & 0 \\ 0 & 1 & 0 & t_2 - t_1 & 0 & (t_2 - t_1)^2/2 \\ 0 & 0 & 1 & 0 & t_2 - t_1 & 0 \\ 0 & 0 & 0 & 1 & 0 & t_2 - t_1 \\ 0 & 0 & 0 & 0 & 1 & 0 \\ 0 & 0 & 0 & 0 & 0 & 1 \end{bmatrix}$$

$$H = \begin{bmatrix} 1 & 0 & 0 & 0 & 0 & 0 \\ 0 & 1 & 0 & 0 & 0 & 0 \end{bmatrix}$$

$$R = \begin{bmatrix} 0.1 & 0 \\ 0 & 0.1 \end{bmatrix}$$

$$Q = 10^{-3} * \begin{bmatrix} 1 & 0 & 0 & 0 & 0 & 0 \\ 0 & 1 & 0 & 0 & 0 & 0 \\ 0 & 0 & 1 & 0 & 0 & 0 \\ 0 & 0 & 0 & 1 & 0 & 0 \\ 0 & 0 & 0 & 0 & 1 & 0 \\ 0 & 0 & 0 & 0 & 0 & 1 \end{bmatrix}$$

, respectively.

The measured trajectory is

$Z = \{(x_1, y_1), (x_2, y_2), ..., (x_n, y_n)\}$

1: **Predict:**

2: Predicted state estimate: $X_k = F * X_0$;

3: Predicted error covariance: $P_k = F * P_0 * F' + Q$.

4: **Update:**

5: Measurement residual: $Y_k = Z - H * X_k$;

6: Measurement residual covariance: $S_k = H * Pk * H' + R$;

7: Optimal Kalman gain: $K_k = P_k * H'/S_k$;

8: Updated state estimate: $X_0 = X_k + K_k * Y_k$;

9: Updated estimate covariance: $P_0 = (I - K_k * H) * P_k$.

Algorithm 6: Tracking Algorithm based on Kalman Filter

5.2.4 Simulation and Analysis

In this section, we present simulations on the proposed algorithm. We use GPS to record vehicle moving data as the actual trajectory. The accuracy of GPS data is about 1 meter, and the minimal time interval is 1 second. The actual and filtered trajectories are shown in Fig. 5.6.

Define the *error* as the average distance between the filtered and actual coordinates. In fig.5.7, we find that the more often we observe, the more accurate we can estimate the trajectory. The minimal error is about 3 meters. In Fig. 5.8, we conclude that the flatter the trajectory is, the more error the filter will make.

5.2.5 Conclusion

We have carried out a series of experiments of test reflection characteristics of different materials. Then we proposed an algorithm based on the Kalman filter to detect and track the object that causes the reflection. We compared estimation of trajectory with real trajectory recorded from GPS, which shows the validity of the proposed algorithms.

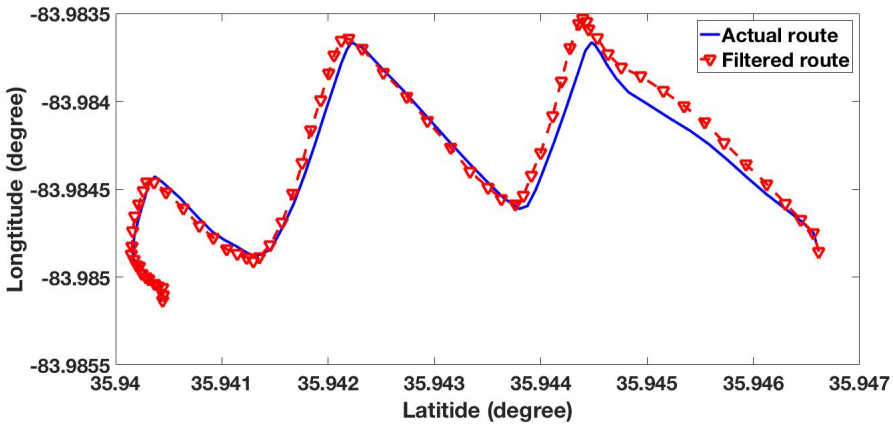


Figure 5.6: Actual and filtered trajectories.

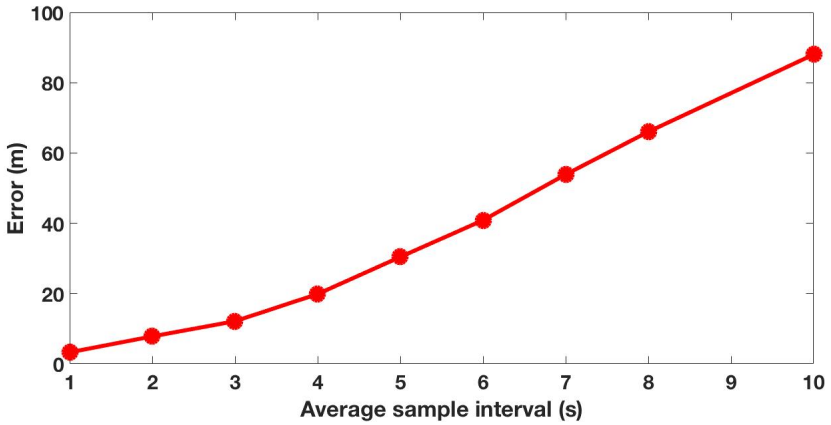


Figure 5.7: Error in term of average sample rate.

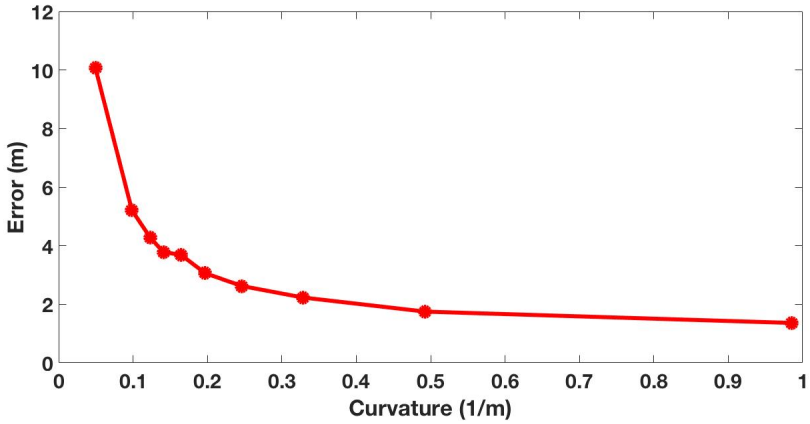


Figure 5.8: Error in term of average sample rate.

5.3 Diffraction

Diffraction is the interference or bending of waves around the corners of an obstacle. It usually happens in visible light propagation. Since the wavelength of mmWave is very close to visible light, we want to find out whether it can be diffracted and transmitted into relatively closed space, just as visible light.

Fig. 5.9 shows the live picture of our experiment environment. The slit is formed by two pieces of stainless steel sheet. The surrounding parts are covered by aluminum foil to prevent extra transmission and reduce multi-path propagation to its minimum.

5.3.1 Single-slit Diffraction

As shown in Fig. 5.10, the process is:

- 60GHz signal is transmitted through a slit.
- The receiver keeps moving circularly in the center of the slit.
- In each position, the corresponding angle and amplitude of the received signal are recorded.

Theoretically, by using the Fraunhofer diffraction [34], the intensity on the receiver can be represented as

$$I(\theta) = I_0 sinc^2\left(\frac{b\pi sin\theta}{\lambda}\right), \tag{5.14}$$

where $I(\theta)$ is the intensity at a given angle, and I_0 is the original intensity, $\lambda = 5mm$ is the wavelength of mmWave, b is the width of the slit, and θ is the angle between the received location and the center of slit.

As a result, the amplitude we receive is

$$A(\theta) = A_0\left|sinc\left(\frac{b\pi sin\theta}{\lambda}\right)\right| \tag{5.15}$$



Figure 5.9: Live picture of single-slit.

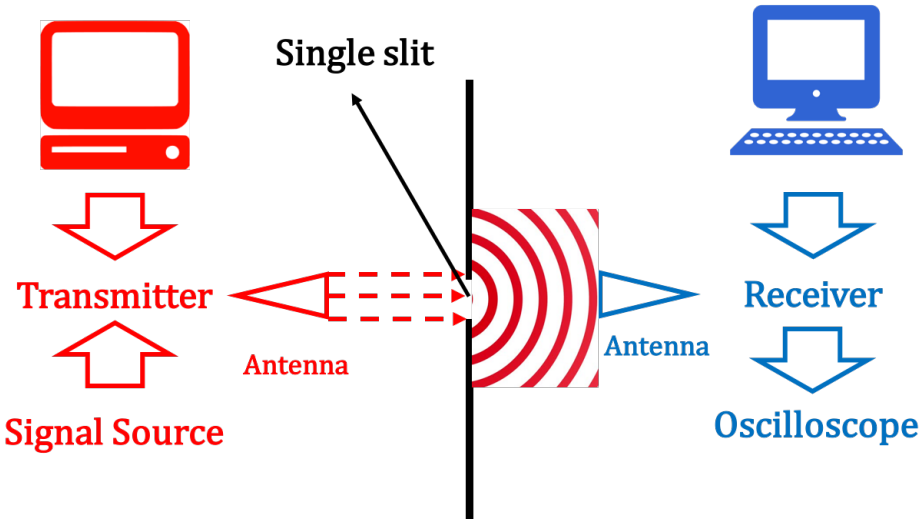


Figure 5.10: Single-slit diffraction experiment setup.

where $A(\theta)$ is the amplitude at a given angle, and A_0 is the original amplitude.

Fig. 5.11 and Fig. 5.12 show that experiment measurement are consistent with theoretical values very well in cases of $b = 10mm$ and $b = 20mm$. However, the minimum amplitude is not zero, which implies some extra transmission signal is received.

5.3.2 Double-slit Interference

As shown in Fig. 5.13, we set the width of both slits as $b = 20mm$, the distance between two slits as $c = 20mm$, and the distance from receiver to slits as $l = 1.5m$.

Since $d > \lambda$, the Fraunhofer diffraction equation gives the intensity of the diffracted light as [34]

$$I(\theta) = 4A_0^2 sinc^2\left(\frac{\pi b sin\theta}{\lambda}\right) cos^2\left(\frac{\pi(b+c)sin\theta}{\lambda}\right) \tag{5.16}$$

Then the amplitude is

$$A(\theta) = 2A_0\left|sinc\left(\frac{\pi b sin\theta}{\lambda}\right) cos\left(\frac{\pi(b+c)sin\theta}{\lambda}\right)\right| \tag{5.17}$$

In Fig. 5.14, experiment records basically agree with the theoretical values, despite the spacing shifting, which is caused by experimental errors. We also notice that the average spacing of the fringes in experiment is a little larger than that in theory, which is because the signal into two slits are not strictly parallel.

5.3.3 Conclusion

We have carried out experiments to verify single-slit and double-slit diffractions of mmWave. Experimental results agree with theoretical values in light wavelength. Hence, the diffraction characteristic of mmWave is very similar to that of visible

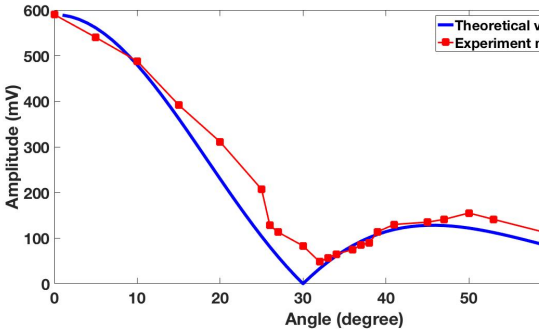


Figure 5.11: Case 1: b=10mm.

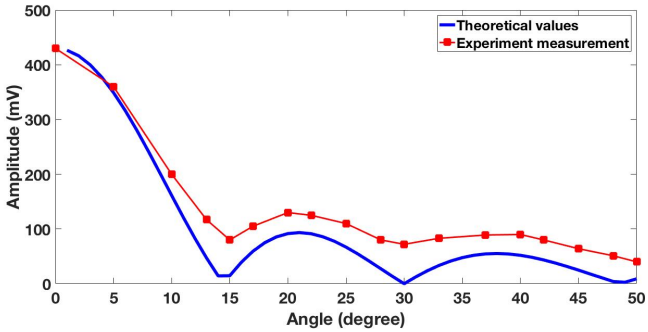


Figure 5.12: Case 2: b=20mm.

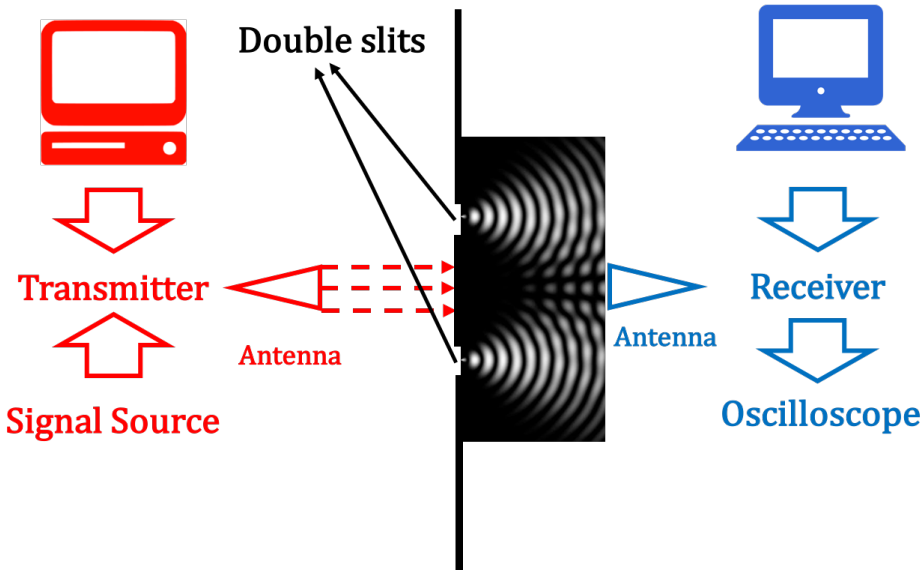


Figure 5.13: Double-slit interference experiment setup.

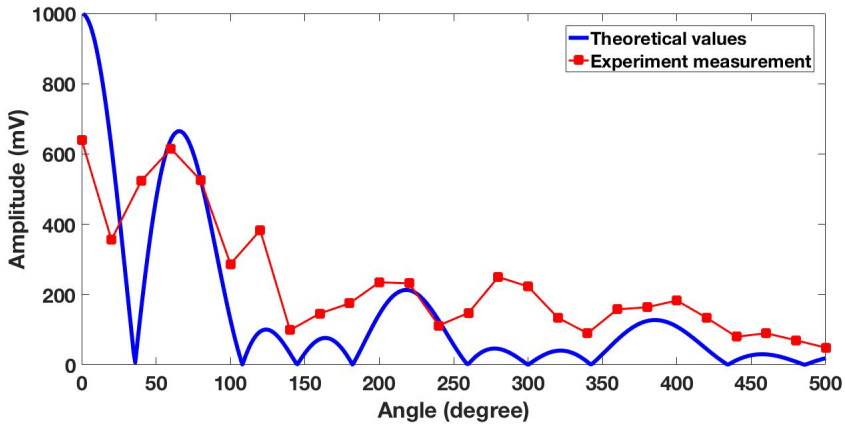


Figure 5.14: Double-slit interference experiment results.

light. It is feasible to establish a reliable wwWave communication in relatively closed space.

Chapter 6

Conclusions and Future Work

6.1 Conclusions

The purpose of this thesis is to benefit from weaknesses of mmWave communication. It mainly covers two topics in the mmWave communication: object tracking via blockage and wind sensing. At the beginning of the thesis, we introduce a brief history of mmWave and its unique characteristics. The challenges of mmWave in telecommunication is discussed. Then, to verify the source of problem, we build a high directional mmWave communication testbed.

In order to study the blockage effect in mmWave communication, we carry out a series of exhaustive experiments. For single object tracking, we propose two hypotheses to simulate human being's walking behavior: shortest path and minimum velocity variance. For multiple objects tracking, we formulate the problem and convert it to an intuitive geometric problem. The corresponding algorithms are presented and analyzed. The estimation of trajectory compared with GPS based real trajectory shows their validity.

The second topic is related to remote sensing. In practice, a lot of 5G devices are deployed outdoor and inevitably affected by wind. We carry out experiments to verify the Doppler effect caused by wind in the millimeter wave band. The results

have shown that a frequency oscillation can be easily detected in the demodulated signal. Based on this, we propose mathematical models to establish the link between frequency and wind speed, and propose an algorithm to calculate wind velocity. We carry out an experiment in the 60GHz band to demonstrate the theoretical prediction, and the outcome matches the theoretical model quite well.

Finally, we investigate other optical-like characteristics of mmWave: reflection and diffraction. An oscillation phenomenon is observed in experiments. We build a mathematical model and propose an algorithm to track moving object in real time. We also carry out experiments of single-slit and double-slit diffraction. The experimental measurements basically matches theoretical value, which indicates that we can use reflection and diffraction to bypass obstacles and establish extra communication link just as visible light.

6.2 Future Work

In chapter 3, we proposed two hypotheses. To get closer to human walking behavior, we plan to propose more advanced hypotheses, including: person prefers a constant walking velocity in a short time.

In chapter 4, we estimated wind velocity in ideal situation. But noise could be extremely high in practice. In the future, we want to study how the noise can affect the measurement of variance of frequency.

In chapter 5, we verified the diffraction phenomenon in mmWave communication. In the future, we plan to study further and propose reliable channel model and algorithm to establish commutation link in relatively closed space.

Bibliography

[1] Abdu, F. J., Zhang, Y., Fu, M., Li, Y., and Deng, Z. (2021). Application of deep learning on millimeter-wave radar signals: A review. *Sensors*, 21(6):1951. 9

[2] Afsar, M. N. (1984). Dielectric measurements of millimeter-wave materials. *IEEE Transactions on Microwave Theory and Techniques*, 32(12):1598–1609. 3

[3] Al-Saman, A., Cheffena, M., Elijah, O., Al-Gumaei, Y. A., Abdul Rahim, S. K., and Al-Hadhrami, T. (2021). Survey of millimeter-wave propagation measurements and models in indoor environments. *Electronics*, 10(14):1653. 9

[4] Aldubaikhy, K., Wu, W., Zhang, N., Cheng, N., and Shen, X. (2020). mmwave ieee 802.11 ay for 5g fixed wireless access. *IEEE Wireless Communications*, 27(2):88–95. 1

[5] Alkhateeb, A., Beltagy, I., and Alex, S. (2018). Machine learning for reliable mmwave systems: Blockage prediction and proactive handoff. In *2018 IEEE Global conference on signal and information processing (GlobalSIP)*, pages 1055–1059. IEEE. 6

[6] Allen, K. C. (1994). Building penetration loss measurements at 900 mhz, 11.4 ghz, and 28.8 ghz. Technical report, Institute for Telecommunication Sciences. 21

[7] Alrabeiah, M. and Alkhateeb, A. (2020). Deep learning for mmwave beam and blockage prediction using sub-6 ghz channels. *IEEE Transactions on Communications*, 68(9):5504–5518. 6

[8] An, X., Sum, C.-S., Prasad, R. V., Wang, J., Lan, Z., Wang, J., Hekmat, R., Harada, H., and Niemegeers, I. (2009). Beam switching support to resolve link-blockage problem in 60 ghz wpans. In *Personal, Indoor and Mobile Radio Communications, 2009 IEEE 20th International Symposium on*, pages 390–394. IEEE. 22

[9] Andrews, J. G., Bai, T., Kulkarni, M. N., Alkhateeb, A., Gupta, A. K., and Heath, R. W. (2016). Modeling and analyzing millimeter wave cellular systems. *IEEE Transactions on Communications*, 65(1):403–430. 7

[10] Barowski, J., Rolfes, I., and Baer, C. (2017). Real-time imaging system for millimeter wave synthetic aperture radar sensors. In *Proc. of IEEE MTT-S International Microwave Bio Conference*. IEEE. 57

[11] Basar, E., Yildirim, I., and Kilinc, F. (2021). Indoor and outdoor physical channel modeling and efficient positioning for reconfigurable intelligent surfaces in mmwave bands. *IEEE Transactions on Communications*, 69(12):8600–8611. 6

[12] Beck, C., Ng, H. J., Agethen, R., PourMousavi, M., Forstner, H. P., Wojnowski, M., Pressel, K., Weigel, R., Hagelauer, A., and Kissinger, D. (2016). Industrial mmwave radar sensor in embedded wafer-level bga packaging technology. *IEEE Sensors Journal*, 16(17):6566–6578. 2

[13] Berclaz, J., Fleuret, F., Turetken, E., and Fua, P. (2011). Multiple object tracking using k-shortest paths optimization. *IEEE transactions on pattern analysis and machine intelligence*, 33(9):1806–1819. 23

[14] Bernardin, K. and Stiefelhagen, R. (2008). Evaluating multiple object tracking performance: the clear mot metrics. *EURASIP Journal on Image and Video Processing*, 2008(1):246309. 23

[15] Boresi, A. P., Schmidt, R. J., and Sidebottom, O. M. (1985). *Advanced Mechanics of Materials*, volume 6. Wiley New York et al. 58, 59

[16] Choi, J., Va, V., Gonzalez-Prelcic, N., Daniels, R., Bhat, C. R., and Heath, R. W. (2016). Millimeter-wave vehicular communication to support massive automotive sensing. *IEEE Communications Magazine*, 54(12):160–167. 57

[17] Collonge, S., Zaharia, G., and Zein, G. E. (2004). Influence of the human activity on wide-band characteristics of the 60 ghz indoor radio channel. *IEEE Transactions on Wireless Communications*, 3(6):2396–2406. 23

[18] David, H. A. and Nagaraja., H. N. (2005). *Order Statistics, Third Edition*. John Wiley & Sons. 38, 39

[19] Dong, M. and Kim, T. (2018). Interference analysis for millimeter-wave networks with geometry-dependent first-order reflections. *IEEE Transactions on Vehicular Technology*, 67(12):12404–12409. 8

[20] Emerson, D. (1997). The work of jagadis chandra bose: 100 years of mm-wave research. In *1997 IEEE MTT-S International Microwave Symposium Digest*, volume 2, pages 553–556. IEEE. 16

[21] Feng, W., Wang, Y., Lin, D., Ge, N., Lu, J., and Li, S. (2017). When mmwave communications meet network densification: A scalable interference coordination perspective. *IEEE Journal on Selected Areas in Communications*, 35(7):1459–1471. 4

[22] Frey, T. L. (1999). The effects of the atmosphere and weather on the performance of a mm-wave communication link. *Applied Microwave and Wireless*, 11:76–81. 20

[23] Friis, H. T. (1946). A note on a simple transmission formula. *Proceedings of the IRE*, 34(5):254–256. 17

[24] Gapeyenko, M., Samuylov, A., Gerasimenko, M., Moltchanov, D., Singh, S., Akdeniz, M. R., Aryafar, E., Himayat, N., Andreev, S., and Koucheryavy, Y. (2017). On the temporal effects of mobile blockers in urban millimeter-wave cellular scenarios. *IEEE Transactions on Vehicular Technology*, 66(11):10124–10138. 8

[25] Giordani, M., Zanella, A., and Zorzi, M. (2017). Millimeter wave communication in vehicular networks: Challenges and opportunities. In *2017 6th International Conference on Modern Circuits and Systems Technologies (MOCAST)*, pages 1–6. IEEE. 9

[26] Hasch, J., Topak, E., Schnabel, R., Zwick, T., Weigel, R., and Waldschmidt, C. (2012). Millimeter-wave technology for automotive radar sensors in the 77 ghz frequency band. *IEEE Transactions on Microwave Theory and Techniques*, 60(3):845–860. 10, 23, 57

[27] He, L., Fang, X., Li, H., Li, C., and Liu, Y. (2016). An mmwave beamforming scheme for disaster detection in high speed railway. In *2016 IEEE/CIC International Conference on Communications in China (ICCC)*, pages 1–6. IEEE. 6

[28] Heath, R. W., Gonzalez-Prelcic, N., Rangan, S., Roh, W., and Sayeed, A. M. (2016). An overview of signal processing techniques for millimeter wave mimo systems. *IEEE journal of selected topics in signal processing*, 10(3):436–453. 3

[29] Hsu, C.-Y., Ahuja, A., Yue, S., Hristov, R., Kabelac, Z., and Katabi, D. (2017). Zero-effort in-home sleep and insomnia monitoring using radio signals. *Proceedings of the ACM on Interactive, Mobile, Wearable and Ubiquitous Technologies*, 1(3):59. 58

[30] Humadi, K. M., Zhu, W.-P., and Ajib, W. (2020). Performance analysis of adaptive modulation for millimeter wave cellular systems. In *2020 IEEE 91st Vehicular Technology Conference (VTC2020-Spring)*, pages 1–5. IEEE. 5

[31] Hussain, M., Scalabrin, M., Rossi, M., and Michelusi, N. (2020). Mobility and blockage-aware communications in millimeter-wave vehicular networks. *IEEE Transactions on Vehicular Technology*, 69(11):13072–13086. 9

[32] Ikram, M. Z. and Ali, M. (2013). 3-d object tracking in millimeter-wave radar for advanced driver assistance systems. In *Global Conference on Signal and Information Processing (GlobalSIP), 2013 IEEE*, pages 723–726. IEEE. 23

[33] Jacob, M., Priebe, S., Maltsev, A., Lomayev, A., Erceg, V., and Kürner, T. (2011). A ray tracing based stochastic human blockage model for the ieee 802.11 ad 60 ghz channel model. In *Antennas and Propagation (EUCAP), Proceedings of the 5th European Conference on*, pages 3084–3088. IEEE. 23

[34] Jenkins, F. and White, H. (1976). *Fundamentals of Optics*. Electromagnetics Series. McGraw-Hill. 88, 90

[35] Jin, F., Sengupta, A., Cao, S., and Wu, Y.-J. (2020). Mmwave radar point cloud segmentation using gmm in multimodal traffic monitoring. In *2020 IEEE International Radar Conference (RADAR)*, pages 732–737. IEEE. 7

[36] Johnson, A. E. and Hebert, M. (1999). Using spin images for efficient object recognition in cluttered 3d scenes. *IEEE Transactions on pattern analysis and machine intelligence*, 21(5):433–449. 23

[37] Juneja, S., Pratap, R., and Sharma, R. (2021). Semiconductor technologies for 5g implementation at millimeter wave frequencies–design challenges and current state of work. *Engineering Science and Technology, an International Journal*, 24(1):205–217. 3

[38] Kameyama, S., Ando, T., Asaka, K., Hirano, Y., and Wadaka, S. (2007). Compact all-fiber pulsed coherent doppler lidar system for wind sensing. *Applied Optics*, 46(11):1953–1962. 58

[39] Khafaji, A., Saadane, R., El Abbadi, J., and Belkasmi, M. (2008). Ray tracing technique based 60 ghz band propagation modelling and influence of people shadowing. *World Academy of Science, Engineering and Technology*. 23

[40] Lathi, B. P. and Ding, Z. (2018). *Modern Digital and Analog Communication*. Oxford University Press. 62

[41] Lawrence, T., Wilson, D., Craven, C., Jones, I., Huffaker, R., and Thomson, J. (1972). A laser velocimeter for remote wind sensing. *Review of Scientific Instruments*, 43(3):512–518. 58

[42] Li, H. (2019). Sensing by leveraging millimeter wave communication networks. In *2019 IEEE Global Communications Conference (GLOBECOM)*, pages 1–6. IEEE. 80

[43] Li, L. and Li, H. (2018). Positioning via spectrum sensing using multidimensional scaling and metric learning with an application in millimeter wave networks. In *2018 IEEE International Conference on Communications Workshops (ICC Workshops)*, pages 1–6. IEEE. 58

[44] Liao, A., Gao, Z., Wu, Y., Wang, H., and Alouini, M.-S. (2017). 2d unitary esprit based super-resolution channel estimation for millimeter-wave massive mimo with hybrid precoding. *IEEE Access*, 5:24747–24757. 11

[45] Lien, J., Gillian, N., Karagozler, M. E., Amihood, P., Schwesig, C., Olson, E., Raja, H., and Poupyrev, I. (2016). Soli: Ubiquitous gesture sensing with millimeter wave radar. *ACM Transactions on Graphics (TOG)*, 35(4):1–19. 10

[46] Lowe, D. G. (1999). Object recognition from local scale-invariant features. In *Computer vision, 1999. The proceedings of the seventh IEEE international conference on*, volume 2, pages 1150–1157. Ieee. 23

[47] Lowe, D. G. (2001). Local feature view clustering for 3d object recognition. In *Computer Vision and Pattern Recognition, 2001. CVPR 2001. Proceedings of the 2001 IEEE Computer Society Conference on*, volume 1, pages I–I. IEEE. 23

[48] Lu, J. S., Steinbach, D., Cabrol, P., and Pietraski, P. (2012). Modeling human blockers in millimeter wave radio links. *ZTE Communications*, 10(4):23–28. 21, 23

[49] Maxwell, J. C. (1865). Viii. a dynamical theory of the electromagnetic field. *Philosophical transactions of the Royal Society of London*, (155):459–512. 16

[50] Oh, J., Thiel, M., and Sarabandi, K. (2014). Wave-propagation management in indoor environments using micro-radio-repeater systems. *IEEE Antennas and Propagation Magazine*, 56(2):76–88. 5

[51] Palizban, N., Szyszkowicz, S., and Yanikomeroglu, H. (2017). Automation of millimeter wave network planning for outdoor coverage in dense urban areas using wall-mounted base stations. *IEEE Wireless Communications Letters*, 6(2):206–209. 5

[52] Patel, M. R. (2005). *Wind and Solar Power Systems: Design, Analysis, and Operation*. CRC press. 58, 59

[53] Pegoraro, J. and Rossi, M. (2021). Real-time people tracking and identification from sparse mm-wave radar point-clouds. *IEEE Access*, 9:78504–78520. 7

[54] Piotrowsky, L., Kueppers, S., Jaeschke, T., and Pohl, N. (2022). Distance measurement using mmwave radar: Micron accuracy at medium range. *IEEE Transactions on Microwave Theory and Techniques*, 70(11):5259–5270. 2

[55] Raghavan, V., Akhoondzadeh-Asl, L., Podshivalov, V., Hulten, J., Tassoudji, M. A., Koymen, O. H., Sampath, A., and Li, J. (2019). Statistical blockage modeling and robustness of beamforming in millimeter-wave systems. *IEEE Transactions on Microwave Theory and Techniques*, 67(7):3010–3024. 4, 7, 10

[56] Rappaport, T. S., Y, X., and et al, G. R. M. (2017). Overview of millimeter wave communications for fifth-generation (5g) wireless networks - with a focus on propagation models. *IEEE Transactions on Antennas and Propagation*, 65. 57

[57] Roh, W., Seol, J.-Y., Park, J., Lee, B., Lee, J., Kim, Y., Cho, J., Cheun, K., and Aryanfar, F. (2014). Millimeter-wave beamforming as an enabling technology for

5g cellular communications: Theoretical feasibility and prototype results. *IEEE communications magazine*, 52(2):106–113. 4

[58] Samuylov, A., Gapeyenko, M., Moltchanov, D., Gerasimenko, M., Singh, S., Himayat, N., Andreev, S., and Koucheryavy, Y. (2016). Characterizing spatial correlation of blockage statistics in urban mmwave systems. In *2016 IEEE Globecom Workshops (GC Wkshps)*, pages 1–7. IEEE. 8

[59] Schlemm, E. (2014). Limiting distribution of the maximal distance between random points on a circle: A moments approach. *Statistics & Probability Letters*, 92:132–136. 38

[60] Schwering, F. K., Violette, E. J., and Espeland, R. H. (1988). Millimeter-wave propagation in vegetation: Experiments and theory. *IEEE Transactions on Geoscience and Remote Sensing*, 26(3):355–367. 21

[61] Shi, Q. and Hong, M. (2018). Spectral efficiency optimization for millimeter wave multiuser mimo systems. *IEEE Journal of Selected Topics in Signal Processing*, 12(3):455–468. 5

[62] Shuai, X., Shen, Y., Tang, Y., Shi, S., Ji, L., and Xing, G. (2021). millieye: A lightweight mmwave radar and camera fusion system for robust object detection. In *Proceedings of the International Conference on Internet-of-Things Design and Implementation*, pages 145–157. 2

[63] Siles, G. A., Riera, J. M., and Garcia-del Pino, P. (2015). Atmospheric attenuation in wireless communication systems at millimeter and thz frequencies [wireless corner]. *IEEE Antennas and Propagation Magazine*, 57(1):48–61. 20

[64] Singh, S., Ziliotto, F., Madhow, U., Belding, E., and Rodwell, M. (2009). Blockage and directivity in 60 ghz wireless personal area networks: From cross-layer model to multihop mac design. *IEEE Journal on Selected Areas in Communications*, 27(8). 22

[65] Steele, J. M. (2004). *Cauchy-Schwartz Master Class*. Cambridge University Press. 39

[66] Sturm, C. and Wisbeck, W. (2011). Waveform design and signal processing aspects for fusion of wireless communications and radar sensing. *Proc. of IEEE*, 99(7). 57

[67] Tariq, M. H., Chondroulis, I., Skartsilas, P., Babu, N., and Papadias, C. B. (2020). mmwave massive mimo channel measurements for fixed wireless and smart city applications. In *2020 IEEE 31st Annual International Symposium on Personal, Indoor and Mobile Radio Communications*, pages 1–6. IEEE. 8

[68] Topfer, F. and Oberhammer, J. (2015). Millimeter-wave tissue diagnosis: The most promising fields for medical applications. *IEEE Microwave Magazine*, 16(4):97–113. 2

[69] Vahidpour, M. and Sarabandi, K. (2012). Millimeter-wave doppler spectrum and polarimetric response of walking bodies. *IEEE Transactions on Geoscience and Remote Sensing*, 50(7):2866–2879. 10

[70] Venugopal, K. and Heath, R. W. (2016). Millimeter wave networked wearables in dense indoor environments. *IEEE Access*, 4:1205–1221. 9

[71] Virk, U. T. and Haneda, K. (2019). Modeling human blockage at 5g millimeter-wave frequencies. *IEEE Transactions on Antennas and Propagation*, 68(3):2256–2266. 7

[72] Vuppala, S., Biswas, S., and Ratnarajah, T. (2016). An analysis on secure communication in millimeter/micro-wave hybrid networks. *IEEE transactions on communications*, 64(8):3507–3519. 6

[73] Wang, F., Wang, H., Feng, H., and Xu, X. (2016). A hybrid communication model of millimeter wave and microwave in d2d network. In *2016 IEEE 83rd vehicular technology conference (VTC Spring)*, pages 1–5. IEEE. 6

[74] Wang, T., Zheng, N., Xin, J., and Ma, Z. (2011). Integrating millimeter wave radar with a monocular vision sensor for on-road obstacle detection applications. *Sensors*, 11(9):8992–9008. 6

[75] Wang, X., Kong, L., Kong, F., Qiu, F., Xia, M., Arnon, S., and Chen, G. (2018). Millimeter wave communication: A comprehensive survey. *IEEE Communications Surveys & Tutorials*, 20(3):1616–1653. 17

[76] Wei, T. and Zhang, X. (2015). mtrack: High-precision passive tracking using millimeter wave radios. In *Proceedings of the 21st Annual International Conference on Mobile Computing and Networking*, pages 117–129. 10, 23

[77] Wu, S., Alrabeiah, M., Hredzak, A., Chakrabarti, C., and Alkhateeb, A. (2021). Deep learning for moving blockage prediction using real millimeter wave measurements. *arXiv preprint arXiv:2101.06886*. 6

[78] Yang, C., Duraiswami, R., and Davis, L. (2005). Fast multiple object tracking via a hierarchical particle filter. In *Computer Vision, 2005. ICCV 2005. Tenth IEEE International Conference on*, volume 1, pages 212–219. IEEE. 23

[79] Yao, Y., Liu, C., Zhang, H., Yan, B., Jian, P., Wang, P., Du, L., Chen, X., Han, B., and Fang, Z. (2022). Fall detection system using millimeter-wave radar based on neural network and information fusion. *IEEE Internet of Things Journal*, 9(21):21038–21050. 11

[80] Yates, R. D. and Goodman, D. J. (2014). *Probability and stochastic processes: a friendly introduction for electrical and computer engineers*. John Wiley & Sons. 41

[81] You, L., Gao, X., Li, G. Y., Xia, X.-G., and Ma, N. (2017). Bdma for millimeter-wave/terahertz massive mimo transmission with per-beam synchronization. *IEEE Journal on Selected Areas in Communications*, 35(7):1550–1563. 11

[82] Yu, L., Zhang, J., Zhang, Y., Li, X., and Liu, G. (2022). Long-range blockage prediction based on diffraction fringe characteristics for mmwave communications. *IEEE Communications Letters*, 26(7):1683–1687. 8

[83] Yu, X., Zhang, J., Haenggi, M., and Letaief, K. B. (2017). Coverage analysis for millimeter wave networks: The impact of directional antenna arrays. *IEEE Journal on Selected Areas in Communications*, 35(7):1498–1512. 17

[84] Yujiri, L., Shoucri, M., and Moffa, P. (2003). Passive millimeter-wave imaging. *IEEE Microwave Magazine*, 47. 57

[85] Zavorotny, V. U. and Voronovich, A. G. (2000). Scattering of gps signals from the ocean with wind remote sensing application. *IEEE Transactions on Geoscience and Remote Sensing*, 38(2):951–964. 58

[86] Zhang, F., Wu, C., Wang, B., and Liu, K. R. (2020). mmeye: Super-resolution millimeter wave imaging. *IEEE Internet of Things Journal*, 8(8):6995–7008. 2

[87] Zhang, J., Ge, X., Li, Q., Guizani, M., and Zhang, Y. (2016). 5g millimeter-wave antenna array: Design and challenges. *IEEE Wireless communications*, 24(2):106–112. 3

[88] Zhang, J., Ge, X., Li, Q., Guizani, M., and Zhang, Y. (2017). 5g millimeter-wave antenna array: Design and challenges. *IEEE Wireless Communications*, 24(2):106–112. 10

[89] Zhang, Q., Saad, W., and Bennis, M. (2019a). Reflections in the sky: Millimeter wave communication with uav-carried intelligent reflectors. In *2019 IEEE Global Communications Conference (GLOBECOM)*, pages 1–6. IEEE. 5

[90] Zhang, Z., Bao, J., Fan, Y., and Li, H. (2018a). Tracking via blocking in millimeter wave communication networks. In *2018 IEEE International Conference on Communications (ICC)*, pages 1–6. 13, 22, 75

[91] Zhang, Z., Bao, J., Fan, Y., and Li, H. (2018b). Tracking via blocking in millimeter wave communication networks. *2018 IEEE International Conference on Communications (ICC)*, pages 1–6. 58

[92] Zhang, Z., Bao, J., Fan, Y., and Li, H. (2019b). Wind sensing by millimeter wave communications. In *2019 IEEE International Symposium on Dynamic Spectrum Access Networks (DySPAN)*, pages 1–6. 13, 57

[93] Zhang, Z. and Li, H. (2017). Object tracking via blocking in millimeter wave communications: A blessing misfortune. In *IEEE International Conference on Communications*, page submitted. IEEE. 47

[94] Zhang, Z., Li, L., Fan, Y., and Li, H. (2018c). Object tracking via blocking in millimeter wave communications: A blessing misfortune. In *2018 IEEE International Conference on Communications (ICC)*, pages 1–6. IEEE. 13, 22, 58

[95] Zhao, H., Mayzus, R., Sun, S., Samimi, M., Schulz, J. K., Azar, Y., Wang, K., Wong, G. N., Gutierrez, F., and Rappaport, T. S. (2013). 28 ghz millimeter wave cellular communication measurements for reflection and penetration loss in and around buildings in new york city. In *2013 IEEE international conference on communications (ICC)*, pages 5163–5167. IEEE. 21

Vita

Vita goes here...